

## Dendritic cells enter lymph vessels by hyaluronan-mediated docking to the endothelial receptor LYVE-1

Louise A. Johnson<sup>1</sup>, Suneale Banerji<sup>1</sup>, William Lawrance<sup>1</sup>, Uzi Gileadi<sup>1</sup>, Gennaro Prota<sup>1</sup>, Kayla A. Holder<sup>1</sup>, Yaowaluck M. Roshorm<sup>2</sup>, Tomáš Hanke<sup>3,4</sup>, Vincenzo Cerundolo<sup>1</sup>, Nicholas W. Gale<sup>5</sup>, David G. Jackson<sup>1</sup>

<sup>1</sup>MRC Human Immunology Unit, University of Oxford, Weatherall Institute of Molecular Medicine, John Radcliffe Hospital, Headington, Oxford, OX3 9DS, U.K.

<sup>2</sup>King Monkut's University of Technology, Thonburi, Thailand. <sup>3</sup>The Jenner Institute, University of Oxford, Old Road Campus Research Building, Roosevelt Drive, Oxford, OX3 7DQ, U.K. <sup>5</sup>Regeneron Pharmaceuticals, Tarrytown, NY, USA.

Correspondence should be addressed to D. G. J. (david.jackson@imm.ox.ac.uk) or

L.A.J. (louise.johnson@imm.ox.ac.uk)

14   **Abstract**

15   Trafficking of tissue dendritic cells (DCs) *via* lymph is critical for generating cellular  
16   immune responses in draining lymph nodes. Here, we showed that DCs docked to the  
17   basolateral surface of lymphatic vessels and transited to the lumen through  
18   hyaluronan-mediated interactions with the lymph-specific endothelial receptor  
19   LYVE-1, in dynamic transmigratory cup-like structures. Furthermore, we showed that  
20   targeted *Lyve1* gene deletion, antibody blockade or depletion of the DC hyaluronan  
21   coat not only delayed lymphatic trafficking of dermal DCs but also blunted their  
22   capacity to prime CD8<sup>+</sup> T-cell responses in skin-draining lymph nodes. Our findings  
23   uncovered a previously unknown function for LYVE-1 and showed that transit  
24   through the lymphatic network was initiated by recognition of leukocyte-derived  
25   hyaluronan.

26



## 27 **Introduction**

28 Afferent lymphatic vessels provide essential conduits for transporting antigen-  
29 presenting dendritic cells (DCs), from the periphery to draining lymph nodes (LNs).  
30 During normal homeostasis, low level trafficking of immature tissue resident DCs  
31 allows for local immune surveillance, whereas in inflammation and infection, the  
32 enhanced migration of both resident and monocyte-derived DCs allows for efficient  
33 generation of primary immune responses to invading pathogens<sup>1</sup>.

34 The first key steps in this chain of events are migration of DCs within the  
35 tissue interstitium towards initial lymphatic capillaries, transit across endothelium into  
36 the vessel lumen, and crawling in the direction of downstream lymphatic collectors<sup>2</sup>.  
37 These processes are directed by a combination of interstitial flow<sup>3</sup>, chemotaxis and  
38 haptotaxis in response to gradients of lymphatic endothelial-derived chemokines  
39 including CCL21, CXCL12 and CX3CL1 that engage with their cognate leukocyte  
40 receptors CCR7, CXCR4 and CX3CR1<sup>4-11</sup> and semaphorins<sup>12</sup>. However, the  
41 mechanisms underlying DC transit across lymphatic endothelium are poorly  
42 understood.

43 It is now appreciated that initial lymphatic capillaries have specialized inter-  
44 endothelial junctions distinct from those of blood capillaries<sup>13</sup>. These comprise loose,  
45 overlapping flaps anchored on their sides by “buttons” containing the adherens  
46 junction molecule VE-cadherin and tight junction-associated proteins such as claudins  
47 and ZO-1. Notably, the openings formed by these flaps constitute 1 – 2  $\mu$ m valve-like  
48 portals that are just large enough for migrating leukocytes to enter. Indeed,  
49 endogenous class II Major Histocompatibility Complex positive (MHCII<sup>+</sup>) DCs have  
50 been observed to squeeze through such junctions into lymphatic capillaries<sup>13</sup>.  
51 Nevertheless, the interactions between DCs and lymphatic endothelium that facilitate  
52 transit remain unknown. Previous studies have reported transit does not involve

53 conventional integrin-based adhesion and is instead mediated through contractile  
54 forces<sup>5,14</sup>, whereas others have shown that in inflammation, transit requires  
55 engagement of DC integrins with their endothelial ligands ICAM-1 and VCAM-1<sup>15–</sup>  
56 <sup>17</sup>. Several other candidate adhesion molecules have also been reported to regulate DC  
57 entry to the lymphatics, including CD31, CD99, CD137, L1CAM, ALCAM and the  
58 scavenger receptors CLEVER-1 and Mannose receptor<sup>9,18,19</sup>. However, these are also  
59 expressed in blood vessel endothelium and no adhesion molecules specific to  
60 lymphatic entry have been convincingly described.

61         One particularly abundant component of button-like lymphatic junctions that  
62 has been proposed to mediate leukocyte entry is the lymphatic vessel endothelial  
63 protein LYVE-1, a receptor for the large ubiquitous glycosaminoglycan polymer  
64 hyaluronan (HA), [GlcNAc $\beta$ 1-4GlcUA $\beta$ 1-3]<sub>n</sub><sup>20</sup>. LYVE-1 is present at high density  
65 within the distinctive overlapping junctions of initial lymphatics but largely absent  
66 from the conventional tight junctions of larger collector vessels. Furthermore, LYVE-  
67 1 is closely related to the primary leukocyte HA receptor CD44, which mediates HA-  
68 dependent adhesion and extravasation of leukocytes across inflamed blood vessels<sup>21</sup>.

69         Here we have explored the involvement of LYVE-1 and its ligand HA in the  
70 trafficking of leukocytes within lymphatic vessels. Using *Lyve1*<sup>-/-</sup> mice and function-  
71 blocking mAbs, we showed that efficient lymphatic trafficking of DCs from the  
72 inflamed skin was dependent upon LYVE-1, and that LYVE-1-HA interactions  
73 mediated an initial vessel entry step that was rate-limiting for DC-primed immune  
74 responses in draining lymph nodes. Moreover, we demonstrate that migrating DCs  
75 assembled an endogenous HA surface coat, which enabled docking to the lymphatic  
76 endothelium *via* LYVE-1 within discrete transmigratory cups that enveloped the  
77 transiting DC and facilitated its passage to the vessel lumen. These findings identify  
78 an important immunological function for this widely used lymphatic marker and

79 reveal a previously unidentified role for the LYVE-1-HA interaction, as a regulator of  
80 leukocyte trafficking in the lymphatics.  
81

## 82    **Results**

### 83    ***Lyve1* gene deletion impairs DC migration to skin-draining LNs**

84    To explore the involvement of LYVE-1 in the migration of DCs from the peripheral  
85    tissues to lymph during both normal homeostasis and inflammation, we used a mouse  
86    skin contact-hypersensitivity model, in which sensitization with the chemical allergen  
87    oxazolone induces rapid mobilization of epidermal Langerhans cells and dermal DCs,  
88    and subsequent trafficking to skin-draining LNs that is detectable within 24 h  
89    (**Supplementary Fig. 1a**)<sup>22</sup>. We found a reduction in the numbers of skin-derived  
90    CD11c<sup>+</sup>FITC<sup>+</sup> DCs recovered in draining inguinal and axillary LNs at 6 h and 24 h  
91    post oxazolone-sensitization in *Lyve1*<sup>-/-</sup> BALB/c mice compared to *Lyve1*<sup>+/+</sup>  
92    littermates, which was followed by a compensatory rise in CD11c<sup>+</sup>FITC<sup>+</sup> DC  
93    numbers arriving at LNs at 48 h in the *Lyve1*<sup>-/-</sup> BALB/c mice (**Fig. 1a**). This  
94    interruption in trafficking was highly reproducible and appeared to affect all subsets  
95    of migratory CD11c<sup>+</sup>MHCII<sup>+</sup> FITC<sup>+</sup> DCs, including CD11b<sup>+</sup> DCs, CD103<sup>+</sup> DCs,  
96    EpCAM<sup>+</sup> DCs and Langerin<sup>+</sup> DCs (**Supplementary Fig. 1b-c**). The composition of  
97    leukocyte populations in the LNs of unchallenged *Lyve1*<sup>-/-</sup> and *Lyve1*<sup>+/+</sup> BALB/c mice  
98    was almost identical (**Supplementary Fig 2**), indicating a defect in inflammation-  
99    associated trafficking, rather than the steady-state composition of LNs in the *Lyve1*<sup>-/-</sup>  
100    mice. We also observed a less marked, but statistically significant reduction in DC  
101    accumulation in LNs at 6h post oxazolone-sensitization and a similar, non-significant  
102    trend at 24 h in *Lyve1*<sup>-/-</sup> C57BL/6 mice compared to *Lyve1*<sup>+/+</sup> littermates together with  
103    a rebound at 48h post-sensitization (**Supplementary Fig. 3a-c**), in contrast to the  
104    original analysis of *Lyve1*<sup>-/-</sup> C57BL/6 mice, which failed to detect a migration  
105    defect<sup>23</sup>, probably due to the incomplete nature of those initial studies. However,  
106    similar to the original analysis<sup>23</sup>, we detected no obvious differences in gross  
107    lymphatic vessel or junctional ultrastructure in *Lyve1*<sup>-/-</sup> mice compared to *Lyve1*<sup>+/+</sup>

littermates on either background. These initial results indicate that LYVE-1 contributed to DC migration *via* dermal lymphatics.

#### **Deficient DC entry to afferent dermal lymphatics in *Lyve1*<sup>-/-</sup> mice**

LYVE-1 is expressed on both luminal and basolateral surfaces of lymph vessel endothelium<sup>24</sup>. To investigate whether the delay in DC trafficking between skin and draining inguinal or axillary LNs in *Lyve1*<sup>-/-</sup> mice was due to a defect in initial lymphatic vessel entry or subsequent intraluminal migration, we visualized the transit of bone marrow-derived DCs (BMDCs) through the dermal lymphatics by confocal imaging. In oxazolone-sensitized *Lyve1*<sup>-/-</sup> and *Lyve1*<sup>+/+</sup> littermate mice injected with LPS-activated, CMFDA-labeled BMDCs, the cells were still visible in large numbers near the injection site 24 h post-injection (**Fig. 1c**), in agreement with reports that only approximately 1% of intradermally injected BMDCs reach draining LNs within this time-frame<sup>4</sup>. In *Lyve1*<sup>+/+</sup> BALB/c mice, CMFDA<sup>+</sup> BMDCs were distributed along podoplanin stained dermal lymphatic vessels at 18 h and 24 h (**Fig. 1b, c**) and orthogonal views of z-stacks revealed that the majority of CMFDA<sup>+</sup> cells associated with these lymphatics (85%) were inside the vessel lumen (**Fig. 1c, d**). In contrast, the distribution of CMFDA<sup>+</sup> BMDCs in LYVE-1-deficient mice was largely independent of podoplanin<sup>+</sup> lymphatics at 18 h (**Fig. 1b**), and those associated with podoplanin<sup>+</sup> lymphatics accumulated at the basolateral surface of the vessels with only 22% present in the vessel lumen at 24 h, suggesting that their transit was stalled in the absence of LYVE-1 (**Fig. 1c, d**). Moreover, the number of dermally injected CMFDA<sup>+</sup> BMDCs recovered in skin-draining LNs of oxazolone-sensitized *Lyve1*<sup>-/-</sup> mice ( $3 \times 10^3$ ) was 3-fold lower than in *Lyve1*<sup>+/+</sup> littermates ( $9 \times 10^3$ , **Fig. 1e**), and total lymph node cellularity was 2.5-fold lower ( $1.9 \times 10^6$  in *Lyve1*<sup>-/-</sup> mice compared with  $8 \times 10^5$  in *Lyve1*<sup>+/+</sup> littermates **Fig. 1f**). These results indicate that LYVE-1 contributed to the access of DCs to the vessel lumen.

### 134 **Compromised egress of DCs from *Lyve1*<sup>-/-</sup> dermal explants**

135 We next used short-term (24 h) *ex-vivo* crawl-out assays<sup>25</sup> to investigate DC  
136 trafficking in cultured skin explants from *Lyve1*<sup>-/-</sup> and *Lyve1*<sup>+/+</sup> BALB/c littermates.  
137 These assays measure the numbers of endogenous dermal DCs and epidermal  
138 Langerhans cells migrating from the skin through afferent dermal lymphatics into the  
139 culture medium, following mobilization by IL-18, IL-1 $\beta$  and TNF released within the  
140 excised tissue<sup>26,27</sup>. Freshly excised skin contained similar numbers of resident  
141 CD45<sup>+</sup>MHCII<sup>+</sup> leukocytes in *Lyve1*<sup>-/-</sup> and *Lyve1*<sup>+/+</sup> littermates (**Fig. 2a-b**). However,  
142 following 24 h of *ex vivo* incubation, the number of CD45<sup>+</sup>MHCII<sup>+</sup> cells recovered in  
143 the medium from the *Lyve1*<sup>-/-</sup> explants ( $2 \times 10^3$ ) was 17-fold lower than in *Lyve1*<sup>+/+</sup>  
144 explants ( $3.4 \times 10^4$ ), **Fig. 2c-f**), comprising both CD103<sup>+</sup> and CD11b<sup>+</sup> DC  
145 populations. Overall these results indicate a role for LYVE-1 in the egress of dermal  
146 DCs from mouse skin explants.

### 147 ***DC trafficking involves interaction with LYVE-1 HA-binding domain***

148 We next examined the consequences of blocking LYVE-1 function *in vivo* in  
149 *Lyve1*<sup>+/+</sup> BALB/c mice with a panel of blocking mAbs. We used ‘house-made’ rat  
150 anti-mouse LYVE-1 mAbs (B1/10 and C1/8)<sup>28,29</sup> and commercially available  
151 (mAb2125, R & D Systems) antibodies that bind epitopes within the Link domain of  
152 LYVE-1, which binds HA. All three mAbs bound both soluble LYVE-1 and LYVE-  
153 1-expressed on the surface of transfected Jurkat cells, and blocked binding of purified  
154 high molecular weight HA to LYVE-1 effectively, albeit with different affinities  
155 (mAb 2125 > B1/10 > C1/8) and relative potencies (IC<sub>50</sub> mAb2125 < B1/10 < C1/8;  
156 **Supplementary Fig. 5a-c**). Binding studies using LYVE-1 site-directed mutants and  
157 mapping onto a structure-based LYVE-1 model indicated that the C1/8 and mAb2125  
158 epitopes are most similar to each other and bracket the predicted HA-binding cleft on  
159 the surface of LYVE-1, binding to residues Gln-50 and Asn136<sup>30</sup>, while the epitope of

160 B1/10 appears to lie towards the opposite face, contacting residues Arg-98 and Phe-  
161 100 (**Supplementary Fig. 5d**).

162 The administration of saturating doses of either mAb2125 or C1/8 to  
163 oxazolone-sensitized *LyveI*<sup>+/+</sup> BALB/c mice caused a 5-fold reduction in the number  
164 of endogenous, FITC-labeled (by skin painting), CD11c<sup>+</sup> DCs recovered from the  
165 draining LNs at 24 h (**Fig. 3a**), along with a reduction in both the number of LN  
166 CD45<sup>+</sup> cells and all subsets of CD11c<sup>+</sup>MHCII<sup>+</sup> DCs (**Supplementary Fig. 5e**) in  
167 comparison with *LyveI*<sup>+/+</sup> mice receiving rat IgG. There was no significant reduction  
168 in the numbers of CD11c<sup>+</sup> FITC-labeled DC recovered from the draining LNs of mice  
169 that were administered saturating doses of mAb B1/10 compared to rat IgG treated  
170 controls (**Supplementary Fig. 3a**), suggesting that the discrete epitope within the  
171 LYVE-1 HA-binding surface for this antibody is not involved in DC recruitment.  
172 Reduced accumulation of FITC<sup>+</sup>CD11c<sup>+</sup> DC in the draining LNs of C1/8- and  
173 mAb2125-treated mice was observed after 24h in both the sensitization and challenge  
174 phases of oxazolone hypersensitivity (**Fig. 3a, b**) and was equally effective in both  
175 BALB/c and C57BL/6 mice (**Fig. 3b, c**). Moreover, the inhibitory effects of C1/8 and  
176 mAb2125 on DC migration were sustained over 48 h post oxazolone-sensitization  
177 (**Fig. 3d**), in marked contrast to the transient delay in DC recruitment seen in the  
178 *LyveI*<sup>-/-</sup> mice. These results suggest that DC migration in dermal lymphatics is  
179 mediated by interactions between LYVE-1 and its ligand, HA.

180 We then used confocal microscopy to visualize lymphatic transit in  
181 oxazolone-sensitized BALB/c *LyveI*<sup>+/+</sup> mice injected with the anti-LYVE-1 mAbs  
182 C1/8, B1/10 and mAb2125, 24 h after intradermal transfer of CMFDA-labeled  
183 BMDCs. C1/8 and mAb2125 injections caused an accumulation of these CMFDA  
184 labeled cells at the outer (basolateral) surface of the LYVE-1<sup>+</sup> lymphatic capillaries  
185 compared to rat IgG controls, whereas B1/10 injection had no such effect (**Fig. 3e**).

186 Quantifying confocal images of skin sections indicated fewer than 20% of vessel-  
187 associated CMFDA<sup>+</sup> BMDCs were present within the lumen in C1/8- and mAb2125-  
188 treated mice, whereas > 80% of vessel-associated CMFDA<sup>+</sup> BMDCs were  
189 intraluminal in control IgG or B1/10-treated mice (**Fig. 3f**). In addition, C1/8 and  
190 mAb2125 treatment elicited 5-fold reductions in the number of CMFDA<sup>+</sup> BMDCs  
191 recovered in the draining LNs of oxazolone-sensitized mice at 24 h after intradermal  
192 injection compared to rat IgG controls (**Fig. 3g**).

193 We also investigated the effects of LYVE-1 mAb blockade on endogenous  
194 CD45<sup>+</sup>MHCII<sup>+</sup> DC migration in dermal lymphatics of cultured BALB/c skin explants  
195 using the *ex vivo* crawl-out assay that quantifies the recovery of egressed cells in the  
196 surrounding media (supernatant) after 24 h. Treatment with C1/8 or mAb2125 over  
197 this period caused a significant 1.6-fold reduction in the numbers of CD45<sup>+</sup>MHCII<sup>+</sup>  
198 cells collected from the explant supernatants compared to rat IgG treated controls,  
199 whereas B1/10 had no significant effect (**Fig. 3h**). This was mirrored by a reciprocal  
200 increase in CD45<sup>+</sup>MHCII<sup>+</sup> DC numbers retained within the dermis in C1/8- and  
201 mAb2125-treated explants (**Fig. 3i**), indicating that targeting LYVE-1-HA-interaction  
202 prevents DC exit *via* dermal lymphatics. These results show that disruption of LYVE-  
203 1-HA interactions by LYVE-1 blocking mAbs impaired lymphatic trafficking of DCs  
204 at the point of initial vessel entry, and that similar interference reduced DC egress  
205 from dermal tissue explants.

#### 206 ***LYVE-1*-mediated DC migration promotes LN CD8 T-cell responses**

207 Next, we examined the physiological importance of LYVE-1-mediated DC  
208 trafficking for antigen delivery and cell-mediated immune responses in draining LNs.  
209 We measured the effects of LYVE-1 C1/8 and B1/10 mAb administration on the F5  
210 transgenic CD8<sup>+</sup> T-cell response to influenza virus A/NT/60/68 nucleoprotein (NP)  
211 peptide ASNENDAM<sup>28,31</sup> expressed from a modified vaccinia virus Ankara (MVA)-



212 vectored MVA.HIVA.NP vaccine in C57BL/10 mice. Mice adoptively transferred  
213 (i.v.) with CFSE-labeled F5 T-cells were injected (i.p.) with LYVE-1 mAbs 24 h  
214 before and after intradermal MVA.HIVA.NP vaccination. In this model, peptide is  
215 delivered to LNs through virus uptake by migrating dermal APCs <sup>28</sup> and hence  
216 depends on efficient migration of antigen-loaded DCs through afferent lymphatic  
217 capillaries. Administration of mAb C1/8 reduced the number of proliferating NP-  
218 specific F5 CD8<sup>+</sup> T-cells in the draining cervical LNs by more than 40% compared to  
219 rat IgG treated controls, as determined by CFSE dilution 72h post-challenge, whereas  
220 the LYVE-1 mAb B1/10, which failed to block DC trafficking to skin-draining LNs  
221 had no appreciable effect (**Fig. 4a, b**). Importantly, i.p. injection of C1/8 did not alter  
222 proliferation of F5 T-cells in the spleens of mice immunized intravenously with  
223 MVA.HIVA.NP compared to rat IgG injected controls (**Fig 4c**). Because the spleen  
224 lacks an afferent lymphatic supply, these results indicated that the LYVE-1-HA  
225 blocking mAbs specifically targeted afferent lymphatic trafficking.

226 We also investigated the proliferative response of adoptively transferred (i.v.)  
227 CFSE-labeled ovalbumin-specific OT1 CD8<sup>+</sup> T-cells in the draining LNs of *Lyve1*<sup>-/-</sup>  
228 C57BL/6 and control *Lyve1*<sup>+/+</sup> littermate recipients after intradermal transfer of  
229 BMDCs pulsed with ovalbumin peptide *ex vivo*. We observed a 25% reduction in  
230 numbers of proliferating OT-1 CD8<sup>+</sup> T-cells in the draining cervical nodes of LYVE-  
231 1-deficient mice (44.8%) than in *Lyve1*<sup>+/+</sup> littermates (59.7%) as determined by CFSE  
232 labeling 44 h after transfer of antigen-loaded DCs (**Fig. 4d, e**). Furthermore, OT-1  
233 CD8<sup>+</sup> T-cells transferred into *Lyve1*<sup>-/-</sup> mice exhibited lower expression of the T-cell  
234 activation markers CD25 and CD69 compared to *Lyve1*<sup>+/+</sup> littermate controls (**Fig. 4f**  
235 and data not shown). We could not detect T-cell proliferation or upregulation of  
236 activation markers in non-draining LNs (data not shown). These results indicate that

237 interference with LYVE-1 blocks lymph node T-cell proliferation to dermally  
238 administered peptide antigens.

### 239 ***LYVE-1 engages migrating DCs via their endogenous surface HA***

240 To investigate whether DC entry to lymphatics is modulated by LYVE-1  
241 interaction with HA on the DC surface<sup>32,33</sup>, we first incubated BMDCs with  
242 recombinant biotin-labeled versican G1 domain (bVG1), a high-affinity HA-binding  
243 protein reagent used to detect HA on the surface of cells<sup>34,35</sup>. bVG1 stained  
244 approximately 50% of CD11c<sup>+</sup>MHCII<sup>+</sup> BMDCs, as assessed by confocal microscopy  
245 and flow cytometry (**Fig. 5a-b** and **Supplementary Fig. 4b**). Using a sensitive  
246 competitive ELISA, we also detected HA in whole cell lysates and supernatants of  
247 both immature and LPS-activated BMDCs (**Fig. 5c-d**). Additionally, as assessed by  
248 RT-PCR, BMDCs expressed *HAS2* mRNA, encoding the key hyaluronan synthase  
249 protein<sup>32</sup> (**Fig. 5e**), suggesting a capacity for endogenous HA synthesis. HA was also  
250 detected on human monocyte-derived DCs (MDDCs) (**Fig. 5f-g**), and expression  
251 increased upon LPS-induced maturation (**Fig. 5h**).

252 To assess whether HA was expressed by tissue-resident DC populations *in*  
253 *vivo*, we stained ear skin from *Lyve1*<sup>+/+</sup> mice with bVG1, both *in situ* in whole-mount  
254 tissue sections and *ex vivo*, in cytopsin preparations of dermal DCs egressed from *ex*  
255 *vivo* cultured dermal explants collected after 24 h. Because CD11c mAbs failed in  
256 whole-mount staining protocols we used immunostaining with MHCII antibody and  
257 bVG1 in transgenic CD11c-GFP fluorescent DC reporter mice to identify endogenous  
258 CD11c<sup>+</sup> DC (**Supplementary Fig. 6**). HA expression was detected on a large  
259 proportion (67%) of resident CD11c-GFP<sup>+</sup>MHCII<sup>+</sup> DCs *in situ* in skin sections of  
260 these mice (**Fig 5i**), but on all CD11c-GFP<sup>+</sup>MHCII<sup>+</sup> DCs that had egressed after 24 h  
261 from the cultured dermal explants (**Fig. 5j**) indicating an enrichment of the  
262 glycosaminoglycan in this latter population.

263 To directly test if HA is required for DC migration through lymphatic vessels,  
264 we depleted HA from the surface of immature BMDCs by digestion with purified  
265 hyaluronidase (HAase), followed by 72 h treatment in culture with 4-  
266 methylumbelliferone (4-MU), a non-toxic HA synthase inhibitor, to prevent  
267 replenishment by *de novo* re-synthesis during subsequent LPS-induced DC  
268 maturation. Such treatment decreased HA levels to approximately 50% of those in  
269 mock-treated BMDCs and these remained stable 24 h after removal of 4-MU (**Fig. 6a,**  
270 **b**), but did not significantly affect BMDC viability, surface integrin integrity or  
271 expression of CD86 used as a measure of activation (**Supplementary Fig. 4c-e**). To  
272 assess the effects on lymphatic migration, HAase/4-MU- and mock-treated BMDCs,  
273 tagged with Q-dot<sup>®</sup> 585 or Q-dot<sup>®</sup> 655, respectively were co-injected intradermally  
274 into oxazolone-sensitized BALB/c *Lyve1*<sup>+/+</sup> mice, followed by flow cytometry to  
275 assess the numbers of labeled BMDC in the draining LNs. 24 h post-transfer we  
276 recovered up to 3-fold more mock-treated DCs than HAase/4-MU-treated DCs from  
277 the draining LNs, with the latter exhibiting diminished surface expression of HA at  
278 this time point (**Fig. 6c, h**). These data indicate that DCs express HA on their surface  
279 both *in vitro* and *in vivo*, and suggest that HA expression is important for trafficking  
280 *via* afferent lymphatics.

#### 281 ***LYVE-1-HA interactions mediate DC adhesion and transmigration***

282 To define the molecular mechanisms by which LYVE-1 and HA mediate DC  
283 trafficking through lymphatics, we used *in vitro* adhesion and transendothelial  
284 migration assays in which CMFDA-labeled, LPS-matured BMDCs were co-incubated  
285 over monolayers of primary LYVE-1<sup>+</sup> mouse dermal LECs (mLECs) isolated from  
286 BALB/c neonatal skin using immunomagnetic bead selection with LYVE-1 mAb  
287 C1/8<sup>15</sup> and plated on plastic multiwell dishes or on the undersurface of light-opaque  
288 transwell inserts respectively. Co-incubation (2 h) with either mAb2125 or C1/8

289 reduced the number of BMDCs adhering to the mLEC monolayers by 2-fold  
290 compared to isotype-matched control rat IgG, whereas B1/10 had no significant effect  
291 (**Fig. 7a**). Likewise, pre-incubation (2h) with purified hyaluronidase reduced the  
292 number of BMDCs adhering to mLEC monolayers by more than 3-fold compared to  
293 mock treated controls, whereas hyaluronidase treatment of mLECs had no such effect  
294 (**Fig. 7b**), indicating that HA expressed by BMDCs is required for the interaction.  
295 Moreover, inclusion of C1/8 or mAb2125 throughout the duration (12h) of transwell  
296 assay cultures reduced BMDC basolateral-to-luminal transmigration through the  
297 mLEC layer by 2-fold in each case, as assessed by quantitation of fluorescent  
298 (CMFDA) cell numbers, compared to a rat IgG isotype control, while B1/10 showed  
299 no statistically significant effect (**Fig. 7c-e**). These results indicate both DC adhesion  
300 and migration across a LEC monolayer involved LYVE-1 interaction with HA on the  
301 DC surface.

### 302 *Docking to lymphatic endothelium via LYVE-1 transmigratory cups*

303 We next used high-magnification confocal microscopy of BMDCs co-cultured  
304 with primary mLEC monolayers to image the DC:LEC interface and visualize how  
305 the interaction between HA and LYVE-1 facilitates adhesion and transmigration. We  
306 observed that adherent BMDCs docked to the mLEC monolayer surface in discrete  
307 ring-like structures that stained intensely for LYVE-1 (**Fig. 7f**). In z-stack orthogonal  
308 views of the confocal images the ring-like structures appeared as cups that extended  
309 from the endothelium, partly enveloping the adherent DCs (**Fig. 7g, h**). Addition of  
310 C1/8 or mAb2125 to the mLEC-BMDC co-cultures, or HAase pre-treatment of the  
311 BMDCs greatly reduced the number of LYVE-1<sup>+</sup> cups that formed on the mLEC  
312 monolayer surface compared to a rat IgG isotype control (**Fig. 8a-b and**  
313 **Supplementary Fig. 7**), implying that the interaction between LYVE-1 and HA on  
314 the surface of BMDC contributed to the stability of these molecular structures.

315 Similar LYVE-1<sup>+</sup> cups were observed on primary human LEC (hLEC) monolayers  
316 incubated with human MDDCs (Supplementary Fig. 7) and their formation was  
317 inhibited by the addition of the human LYVE-1-HA blocking mAb 891 (**Fig. 8c** and  
318 **Supplementary Fig. 7**). In addition, in frozen skin sections from oxazolone-  
319 sensitized BALB/c mice, HA was closely associated with endogenous MHCII<sup>+</sup> DCs  
320 that were undergoing transmigration into lymphatic vessels (**Fig. 8d**). Finally, in skin  
321 sections from oxazolone-sensitized mice injected intradermally with CMFDA-labeled  
322 BMDCs, these were observed in close contact with LYVE-1<sup>+</sup> protrusions of  
323 lymphatic vessels during diapedesis (**Fig. 8e** and **Supplementary Fig. 8**). These  
324 results show that adhesion of DC to LECs involved formation of LYVE-1+  
325 endothelial “transmigratory cups” through interaction with DC HA, and provide  
326 evidence they form both *in vitro* and *in vivo*.

327

## 328 **Discussion**

329 Here we have revealed that the endothelial HA receptor LYVE-1 is an important  
330 mediator of leukocyte trafficking. LYVE-1 promoted the docking of DCs to  
331 lymphatic vessel endothelium within dynamic endothelial transmigratory cups, by  
332 engaging HA expressed by DC<sup>32</sup>. Using a topical oxazolone-induced model of skin  
333 hypersensitivity in mice, *ex vivo* dermal crawl-out assays, *in vitro* transmigration  
334 assays and fluorescent imaging we showed that genetic deletion of *Lyve1* or  
335 functional disruption by mAbs that interfere with HA-LYVE-1 interactions impaired  
336 early transit of DCs through dermal lymphatic capillaries to draining LNs, by  
337 preventing their interaction with the lymphatic endothelium. Endothelial cup  
338 formation, adhesion and transmigration and LN trafficking were all impaired by  
339 enzymatic removal of HA on the surface of DC and prolonged inhibition of  
340 endogenous HA biosynthesis. Lastly, *Lyve1* gene deletion or antibody blockade

341 significantly reduced the CD8<sup>+</sup> T-cell responses to peptide antigens in the lymph  
342 nodes. As such, LYVE-1-HA interaction mediated a rate-limiting step for DC  
343 lymphatic entry and the initiation of immune responses in skin draining lymph nodes.

344         The transient nature of the DC trafficking defect in *Lyve1*<sup>-/-</sup> mice and the more  
345 sustained effects of LYVE-1 antibody blockade in adult *Lyve1*<sup>+/+</sup> mice, suggest  
346 compensatory mechanisms during embryonic development in mice with genomic  
347 deletion of *Lyve1*, a phenomenon previously suggested for mice deficient in the  
348 primary leukocyte HA receptor CD44<sup>36,37</sup>. Compensation through functional  
349 redundancy may account for the apparently normal phenotype of *Lyve1*<sup>-/-</sup> mice under  
350 normal homeostatic conditions. Moreover, the comparatively short duration of the  
351 trafficking defects in the *Lyve1*<sup>-/-</sup> mice, particularly those on the C57BL/6  
352 background, provides an explanation for the failure to identify an important  
353 trafficking role for LYVE-1 in earlier, more limited studies<sup>23</sup>. Clearly, more detailed  
354 studies of lymphatic trafficking in mice using live imaging and conditional or acute  
355 deletion of *Lyve1* will be required to fully define such phenomena in the future.

356         A function for LYVE-1 as a lymph-specific trafficking receptor is fully  
357 consistent with its segregated expression at the tips of the interdigitating endothelial  
358 junctions of initial lymphatic vessels, which act as hotspots for DC entry *in vivo*<sup>13</sup>.  
359 HA-mediated docking with LYVE-1 at these sites could facilitate DC transmigration  
360 not only through direct adhesion, but also through the local unbuttoning of endothelial  
361 junctions. In support of this view, it is documented that LYVE-1 can transduce signals  
362 for VE-cadherin turnover and endothelial junctional remodeling in LEC-like cell lines  
363 *in vitro*<sup>38</sup>, a process triggered by LYVE-1 mAbs and HA-binding in primary LEC  
364 (Wang *et al*, manuscript in preparation). Although the LEC monolayers used here do  
365 not spontaneously assemble interdigitating button-like junctions during *in vitro*  
366 culture but instead form continuous zipper-like junctions, these are plastic *in vivo* and

367 can transition between the two states according to tissue inflammatory status<sup>39</sup>.  
368 Hence, the LYVE-1<sup>+</sup> transmigratory cups we observed in mouse and human LECs  
369 likely reflect authentic physiological structures. The analogous LYVE-1<sup>+</sup>  
370 membranous protrusions we observed around dermal DCs undergoing vessel entry in  
371 mouse skin lends further credence to this notion.

372         The role played by LYVE-1 in lymphatic trafficking bears comparison with  
373 the closely related leukocyte HA receptor CD44, which mediates lymphocyte and  
374 neutrophil capture from laminar blood flow by engaging HA from the luminal  
375 glycocalyx in inflamed vascular endothelium<sup>40</sup>. Importantly, the avidity of the  
376 CD44:HA interaction necessary for such capture depends on the capacity of HA to  
377 form prior crosslinked complexes with inflammation-associated binding partners such  
378 as TSG-6<sup>41</sup>, or adduct formation with serum-derived HA associated protein (SHAP)  
379 <sup>21,42,43</sup>. In lymphatic vessels, LYVE-1 must instead play a reciprocal role by engaging  
380 HA arrayed on the leukocyte surface. Although we have yet to determine whether  
381 DCs organize this surface HA within similar crosslinked complexes, it is noteworthy  
382 that they can synthesize both TSG-6 and the heavy chain of inter alpha trypsin  
383 inhibitor (IoI) that generates SHAP<sup>44,45</sup>. Moreover, native LYVE-1 has a marked  
384 preference for binding crosslinked HA-TSG-6 complexes, which harness avidity by  
385 inducing receptor surface clustering<sup>46</sup>. This preference is exploited by pathogenic  
386 Group A hemolytic streptococci to bind LYVE-1 through their dense HA surface  
387 capsule for enhanced dissemination to host LNs<sup>47</sup>. Hence the properties of LYVE-1  
388 appear ideally suited for selective docking with cell surface HA assemblages rather  
389 than free ambient HA in the tissue matrix. Indeed, LYVE-1-HA bonds form more  
390 rapidly and rupture more easily than CD44-HA bonds in response to force, despite  
391 their similar binding affinities ( $K_d$  8-100  $\mu$ M) (Bano, F., Banerji, S. Jackson, D.G. and  
392 Richter, R.R. unpublished), in keeping with a role in supporting DC crawling at the

393 lymphatic vessel surface, where lower shear forces are encountered in comparison  
394 with those in venous blood flow<sup>48</sup>.

395 Finally, while our current study highlighted the role of LYVE-1 in mediating  
396 DC entry to dermal lymphatic vessels, it is possible that the receptor also facilitates  
397 trafficking in LNs, where its location in the subcapsular sinus floor would suggest a  
398 role in movement of DCs from lymph to the T-cell-rich paracortex. Both in the  
399 subcapsular sinus floor and in peripheral lymphatics, LYVE-1 likely mediates  
400 migration of a variety of immunomodulatory populations besides DCs. Notably,  
401 monocytes and macrophages also synthesize HA, and human monocyte-derived  
402 macrophages employ LYVE-1 and HA for transmigration across LECs *in vitro*<sup>46</sup>. In  
403 contrast, neutrophils, which exit skin *via* lymph in response to bacterial infection  
404 appear not to utilize LYVE-1 for vessel entry, but rather an unusual  $\beta 2$  integrin- and  
405 lipoxin-mediated mechanism<sup>49,50</sup>. The degree of LYVE-1 involvement may well  
406 depend on the nature and extent of leukocyte HA organization and the particular  
407 choice of vessel sites these cells target for entry.

408 In conclusion, we have shown that the LYVE-1-HA interaction constitutes a  
409 physiologically important axis regulating DC trafficking in lymph. Consequently,  
410 LYVE-1 has the potential as a therapeutic target for limiting inflammation and  
411 associated immune activation.

#### 412 413 **Data availability**

414 The data that support the findings of this study are available from the corresponding  
415 author upon request.

#### 416 **Acknowledgments**

417 This work was supported by the UK Medical Research Council through MRC Human  
418 Immunology Unit core funding and Project Grant MR/L008610/1 to D.G.J. The



419 authors would also like to acknowledge the now deceased M. Puklavec (Sir William  
420 Dunn School of Pathology, Oxford), for his invaluable technical advice on making rat  
421 monoclonal antibodies, and the Wolfson Imaging Centre, Weatherall Institute of  
422 Molecular Medicine, Oxford for use of the fluorescence microscope equipment in this  
423 project. The authors also thank P. Sopp, C. Waugh, K. Clark and S.-A. Clark from the  
424 WIMM Flow Cytometry Facility, for their excellent technical assistance and advice.

#### 425 **Author Contributions**

426 L.A.J. and D.G.J. designed experiments, interpreted the data and wrote the  
427 manuscript, S.B. performed experiments, helped interpret the data and edited the  
428 manuscript. L.A.J., U.G. and G.P. performed experiments and analyzed data, W.L.,  
429 K.A.H., and Y.M.R. performed experiments and provided reagents, T.H., V.C. and  
430 N.W.G. provided critical reagents and helped edit the manuscript.

#### 431 **Competing Financial Interests**

432 The authors declare no competing financial interests.

433

## References

1. Mellman, I. & Steinman, R. M. Dendritic cells: specialized and regulated antigen processing machines. *Cell* **106**, 255–258 (2001).
2. Randolph, G. J., Ivanov, S., Zinselmeyer, B. H. & Scallan, J. P. The Lymphatic System: Integral Roles in Immunity. *Annu. Rev. Immunol.* **35**, annurev-immunol-041015-055354 (2017).
3. Miteva, D. O. *et al.* Transmural flow modulates cell and fluid transport functions of lymphatic endothelium. *Circ Res* **106**, 920–931 (2010).
4. Martín-Fontecha, A. *et al.* Regulation of dendritic cell migration to the draining lymph node: impact on T lymphocyte traffic and priming. *J Exp Med* **198**, 615–621 (2003).
5. Lammermann, T. *et al.* Rapid leukocyte migration by integrin-independent flowing and squeezing. *Nature* **453**, 51–55 (2008).
6. Johnson, L. A. & Jackson, D. G. Inflammation-induced secretion of CCL21 in lymphatic endothelium is a key regulator of integrin-mediated dendritic cell transmigration. *Int Immunol* **22**, 839–849 (2010).
7. Johnson, L. A. & Jackson, D. G. The chemokine CX3CL1 promotes trafficking of dendritic cells through inflamed lymphatics. *J Cell Sci* **126**, 5259–5270 (2013).
8. Kabashima, K. *et al.* CXCL12-CXCR4 engagement is required for migration of cutaneous dendritic cells. *Am J Pathol* **171**, 1249–1257 (2007).
9. Teijeira, A., Russo, E. & Halin, C. Taking the lymphatic route: dendritic cell migration to draining lymph nodes. *Semin Immunopathol* (2014). doi:10.1007/s00281-013-0410-8
10. Russo, E. *et al.* Intralymphatic CCL21 Promotes Tissue Egress of Dendritic Cells through Afferent Lymphatic Vessels. *Cell Rep.* **14**, 1723–1734 (2016).

- 461 11. Weber, M. *et al.* Interstitial dendritic cell guidance by haptotactic chemokine  
462 gradients. *Science* (80-. ). **339**, 328–332 (2013).
- 463 12. Takamatsu, H. *et al.* Semaphorins guide the entry of dendritic cells into the  
464 lymphatics by activating myosin II. *Nat Immunol* **11**, 594–600 (2010).
- 465 13. Baluk, P. *et al.* Functionally specialized junctions between endothelial cells of  
466 lymphatic vessels. *J Exp Med* **204**, 2349–2362 (2007).
- 467 14. Pflücke, H. & Sixt, M. Preformed portals facilitate dendritic cell entry into  
468 afferent lymphatic vessels. *J Exp Med* **206**, 2925–2935 (2009).
- 469 15. Johnson, L. A. *et al.* An inflammation-induced mechanism for leukocyte  
470 transmigration across lymphatic vessel endothelium. *J Exp Med* **203**, 2763–  
471 2777 (2006).
- 472 16. Nitschke, M. *et al.* Differential requirement for ROCK in dendritic cell  
473 migration within lymphatic capillaries in steady-state and inflammation. *Blood*  
474 **120**, 2249–2258 (2012).
- 475 17. Teijeira, A. *et al.* Lymphatic Endothelium Forms Integrin-Engaging 3D  
476 Structures during DC Transit across Inflamed Lymphatic Vessels. *J Invest*  
477 *Dermatol* **133**, 2276–2285 (2013).
- 478 18. Irjala, H. *et al.* Mannose receptor is a novel ligand for L-selectin and mediates  
479 lymphocyte binding to lymphatic endothelium. *J Exp Med* **194**, 1033–1041  
480 (2001).
- 481 19. Salmi, M., Koskinen, K., Henttinen, T., Elimä, K. & Jalkanen, S. CLEVER-1  
482 mediates lymphocyte transmigration through vascular and lymphatic  
483 endothelium. *Blood* **104**, 3849–3857 (2004).
- 484 20. Banerji, S. *et al.* LYVE-1, a new homologue of the CD44 glycoprotein, is a  
485 lymph-specific receptor for hyaluronan. *J. Cell Biol.* **144**, 789–801 (1999).
- 486 21. McDonald, B. & Kubes, P. Interactions between CD44 and Hyaluronan in

- 487 Leukocyte Trafficking. *Front Immunol* **6**, 68 (2015).
- 488 22. Cumberbatch, M., Dearman, R. J., Griffiths, C. E. & Kimber, I. Epidermal  
489 Langerhans cell migration and sensitisation to chemical allergens. *Apmis* **111**,  
490 797–804 (2003).
- 491 23. Gale, N. W. *et al.* Normal lymphatic development and function in mice  
492 deficient for the lymphatic hyaluronan receptor LYVE-1. *Mol Cell Biol* (2006).
- 493 24. Prevo, R., Banerji, S., Ferguson, D. J. P., Clasper, S. & Jackson, D. G. Mouse  
494 LYVE-1 is an endocytic receptor for hyaluronan in lymphatic endothelium. *J.*  
495 *Biol. Chem.* **276**, 19420–19430 (2001).
- 496 25. Stoitzner, P., Romani, N., McLellan, A. & Tripp, C. Isolation of skin dendritic  
497 cells from mouse and man. *Methods Mol. ...* (2010).
- 498 26. Larsen, C. P. *et al.* Migration and maturation of Langerhans cells in skin  
499 transplants and explants. *J Exp Med* **172**, 1483–1493 (1990).
- 500 27. Cumberbatch, M., Dearman, R. J., Antonopoulos, C., Groves, R. W. & Kimber,  
501 I. Interleukin (IL)-18 induces Langerhans cell migration by a tumour necrosis  
502 factor-alpha- and IL-1beta-dependent mechanism. *Immunology* **102**, 323–330  
503 (2001).
- 504 28. Teoh, D., Johnson, L. A., Hanke, T., McMichael, A. J. & Jackson, D. G.  
505 Blocking development of a CD8+ T-cell response by targeting lymphatic  
506 recruitment of antigen presenting cells. *J. Immunol.* **182**, (2009).
- 507 29. Johnson, L. A., Prevo, R., Clasper, S. & Jackson, D. G. Inflammation-induced  
508 uptake and degradation of the lymphatic endothelial hyaluronan receptor  
509 LYVE-1. *J Biol Chem* **282**, 33671–33680 (2007).
- 510 30. Banerji, S., Hide, B. R., James, J. R., Noble, M. E. & Jackson, D. G.  
511 Distinctive properties of the hyaluronan-binding domain in the lymphatic  
512 endothelial receptor Lyve-1 and their implications for receptor function. *J Biol*

513 *Chem* **285**, 10724–10735 (2010).

514 31. Estcourt, M. J., McMichael, A. J. & Hanke, T. Altered primary CD8+ T-cell  
515 response to a modified virus Ankara(MVA)-vectored vaccine in the absence of  
516 CD4+ T-cell help. *Eur J Immunol* **35**, 3460–3467 (2005).

517 32. Mummert, M. E. *et al.* Synthesis and surface expression of hyaluronan by  
518 dendritic cells and its potential role in antigen presentation. *J Immunol* **169**,  
519 4322–4331 (2002).

520 33. Chang, M. Y. *et al.* A rapid increase in macrophage-derived versican and  
521 hyaluronan in infectious lung disease. *Matrix Biol* **34**, 1–12 (2014).

522 34. de la Motte, C. A. & Drazba, J. A. Viewing hyaluronan: imaging contributes to  
523 imagining new roles for this amazing matrix polymer. *J Histochem Cytochem*  
524 **59**, 252–257 (2011).

525 35. Clark, S. J. *et al.* Mapping the differential distribution of glycosaminoglycans  
526 in the adult human retina, choroid, and sclera. *Invest Ophthalmol Vis Sci* **52**,  
527 6511–6521 (2011).

528 36. Schmits, R. *et al.* CD44 regulates hematopoietic progenitor distribution,  
529 granuloma formation, and tumorigenicity. *Blood* **90**, 2217–2233 (1997).

530 37. Protin, U., Schweighoffer, T., Jochum, W. & Hilberg, F. CD44-deficient mice  
531 develop normally with changes in subpopulations and recirculation of  
532 lymphocyte subsets. *J. Immunology* **163**, 4917–4923 (1999).

533 38. Hou, W. H. *et al.* CRSBP-1/LYVE-1 ligands disrupt lymphatic intercellular  
534 adhesion by inducing tyrosine phosphorylation and internalization of VE-  
535 cadherin. *J Cell Sci* **124**, 1231–1244 (2011).

536 39. Yao, L. C., Baluk, P., Srinivasan, R. S., Oliver, G. & McDonald, D. M.  
537 Plasticity of button-like junctions in the endothelium of airway lymphatics in  
538 development and inflammation. *Am J Pathol* **180**, 2561–2575 (2012).

- 539 40. Siegelman, M. H., DeGrendele, H. C. & Estess, P. Activation and interaction of  
540 CD44 and hyaluronan in immunological systems. *J. Leukoc. Biol.* **66**, 315–21  
541 (1999).
- 542 41. Lesley, J. *et al.* TSG-6 modulates the interaction between hyaluronan and cell  
543 surface CD44. *J. Biol. Chem.* **279**, 25745–25754 (2004).
- 544 42. de la Motte, C. a, Hascall, V. C., Drazba, J., Bandyopadhyay, S. K. & Strong,  
545 S. a. Mononuclear leukocytes bind to specific hyaluronan structures on colon  
546 mucosal smooth muscle cells treated with polyinosinic acid:polycytidylic acid:  
547 inter-alpha-trypsin inhibitor is crucial to structure and function. *Am. J. Pathol.*  
548 **163**, 121–133 (2003).
- 549 43. Petrey, A. C. & de la Motte, C. A. Hyaluronan, a crucial regulator of  
550 inflammation. *Front Immunol* **5**, 101 (2014).
- 551 44. Maina, V. *et al.* Coregulation in human leukocytes of the long pentraxin PTX3  
552 and TSG-6. *J. Leukoc. Biol.* **86**, 123–132 (2009).
- 553 45. Chang, M. Y. *et al.* Monocyte-to-macrophage differentiation: Synthesis and  
554 secretion of a complex extracellular matrix. *J. Biol. Chem.* **287**, 14122–14135  
555 (2012).
- 556 46. Lawrance, W., Banerji, S., Day, A. J., Bhattacharjee, S. & Jackson, D. G.  
557 Binding of hyaluronan to the native lymphatic vessel endothelial receptor  
558 LYVE-1 is critically dependent on receptor surface clustering and hyaluronan  
559 organisation. *J Biol Chem* (2016). doi:10.1074/jbc.M115.708305
- 560 47. Lynskey, N. N. *et al.* Rapid Lymphatic Dissemination of Encapsulated Group  
561 A Streptococci via Lymphatic Vessel Endothelial Receptor-1 Interaction. *PLoS*  
562 *Pathog* **11**, e1005137 (2015).
- 563 48. Bano, F., Banerji, S., Howarth, M., Jackson, D. G. & Richter, R. P. A single  
564 molecule assay to probe monovalent and multivalent bonds between

565           hyaluronan and its key leukocyte receptor CD44 under force. *Sci Rep* **6**, (2016).

566   49.   Hampton, H. R., Bailey, J., Tomura, M., Brink, R. & Chtanova, T. Microbe-  
567           dependent lymphatic migration of neutrophils modulates lymphocyte  
568           proliferation in lymph nodes. *Nat Commun* **6**, 7139 (2015).

569   50.   Rigby, D. A., Ferguson, D. J., Johnson, L. A. & Jackson, D. G. Neutrophils  
570           rapidly transit inflamed lymphatic vessel endothelium via integrin-dependent  
571           proteolysis and lipoxin-induced junctional retraction. *J Leukoc Biol* **98**, 897–  
572           912 (2015).

573

574

575 **Figure legends**

576

577 **Fig. 1. Impaired entry of DCs to dermal lymphatic vessels in BALB/c *LyveI*<sup>-/-</sup>**  
578 **mice. (a)** Recovery of endogenous DCs from draining inguinal and axillary LNs at  
579 indicated time intervals after topical application of oxazolone and FITC, as measured  
580 by flow cytometry. Data represent the mean  $\pm$  s.e. (n = 5), from one experiment of  
581 three, with representative dot plots shown. **(b-c)** Entry of CMFDA-labeled BMDCs  
582 (green) into podoplanin<sup>+</sup> (red) afferent lymphatics of *LyveI*<sup>-/-</sup> and *Lyve*<sup>+/+</sup> litter mates,  
583 as observed by confocal microscopy of whole mount sections of ear dermis, either 18  
584 h **(b)** or 24 h **(c)** after topical application of oxazolone and intradermal injection of  
585 BMDCs. Representative images from three separate repeated experiments are shown,  
586 bar = 100 $\mu$ m. **(c)** Images of three-dimensional rendering of z-stacks are shown at low  
587 magnification (250X, left panels), higher magnification (630X, middle panels) and  
588 include orthogonal sections (right panels). **(d)** Numbers of BMDCs inside the lumens  
589 of lymphatic vessels, expressed as a percentage of the number of lymphatic vessel-  
590 associated BMDCs. Data are the mean values  $\pm$  s.e. (n = 5 mice), from one  
591 experiment of three. **(e, f)** Recovery of i.d. injected BMDCs **(e)** and overall cellularity  
592 **(f)** in draining cervical LNs, 24 h after topical application of oxazolone and adoptive  
593 transfer of BMDCs, as measured by flow cytometry. Data represent the mean  $\pm$  s.e. (n  
594 = 5), from one experiment of two. \* P < 0.05; \*\*P < 0.01.

595 **Figure 2. Impaired egress of dermal DCs from *ex vivo* cultured split ear tissue of**  
596 **BALB/c *LyveI*<sup>-/-</sup> mice. (a-d)** Flow cytometric analysis of digested ear tissue from  
597 wild-type *LyveI*<sup>-/-</sup> mice and *Lyve*<sup>+/+</sup> littermates, either freshly resected **(a, b)** or  
598 following *ex vivo* culturing for 24 h **(c, d)**. **(e, f)** Cells that had egressed from the  
599 dermis into the tissue culture medium were also analyzed by flow cytometry. Data



600 shown by representative dot plots (**a, c, e**) and bar-and-whiskers bar charts (**b, d, f**),  
601 mean  $\pm$  s.e. (n= 5) from one experiment of three, \*\*P < 0.01.

602 **Figure 3. Anti-LYVE-1-specific mAbs inhibit *in vivo* trafficking of DCs through**  
603 **dermal lymphatics. (a-b)** Recovery of endogenous DCs in draining LNs, in BALB/c  
604 mice following injections of rat IgG or anti-LYVE-1 mAbs B1/10, C1/8 or mAb2125,  
605 during either sensitization (**a**) or challenge (**b**) of oxazolone/FITC painting. Data  
606 show numbers of CD45<sup>+</sup>FITC<sup>+</sup>CD11c<sup>+</sup> DCs, (n = 5), one experiment of three. (**c**)  
607 Effect of anti-LYVE-1 mAbs on DC trafficking in C57BL/6 mice, 24 h following  
608 oxazolone/FITC painting, with anti-ICAM-1 mAb YN1-1 as a positive control, (n =  
609 4), one experiment of three. (**d**) Recovery of DCs in draining LNs, 6-48 h after  
610 oxazolone/FITC painting in BALB/c mice injected with rat IgG2a or C1/8, (n = 4),  
611 one experiment of two. (**e-f**) Entry of CMFDA-labeled BMDCs (green) into dermal  
612 afferent lymphatics immunostained with rabbit anti-LYVE-1 (blue) following  
613 oxazolone painting, magnification: 630X, bar = 20 $\mu$ m (Rat IgG and B1/10), bar =  
614 50 $\mu$ m (C1/8 and mAb2125) (**e**), expressed as a percentage of lymphatic vessel-  
615 associated BMDCs (**f**), (n = 5), one experiment of three, with representative images.  
616 Arrows indicate BMDCs within lymphatic vessel lumens; arrow-heads indicate  
617 BMDCs restricted to basolateral surfaces of vessels. (**g**) Recovery of BMDCs from  
618 draining LNs, 24 h after injection. (**h, i**) *Ex-vivo* skin crawl-out assays from ear  
619 tissue, showing numbers of egressed DCs (**h**) and remaining dermal DCs (**i**), (n= 5),  
620 one experiment of three. Data expressed as the mean  $\pm$  s.e. *n.s.*, not significant; \*P <  
621 0.05; \*\*P < 0.01.

622 **Figure 4. Disruption of LYVE-1-mediated DC trafficking inhibits primary**  
623 **antigen-specific T-cell responses in skin-draining LNs. (a,b)** Influenza NP-specific  
624 LN CD8<sup>+</sup> T-cell proliferation, in response to dermally injected MVA.HIVA.NP  
625 vaccine in C57BL/10 mice adoptively transferred with F5 transgenic T-cells and

626 injected with LYVE-1 mAbs, as determined by flow cytometry. Data are plotted as  
 627 percentage of dividing F5 tetramer-reactive CD8<sup>+</sup> T-cells **(a)** with representative  
 628 histograms of CFSE fluorescence, indicating levels of LN T-cell activation **(b)**. **(c)**  
 629 Controls showing unaltered spleen CD8<sup>+</sup> F5 T-cell responses in mice injected i.v with  
 630 MVA.HIVA.NP and the indicated LYVE-1 mAbs, as determined by flow cytometry,  
 631 Data are the mean values  $\pm$  s.e. (n = 3) from one experiment of three. *n.s.*, not  
 632 significant; \*P < 0.05. **(d,e)** Ovalbumin-specific LN CD8<sup>+</sup> T-cell responses elicited by  
 633 peptide (SIINFEKL)-pulsed BMDCs after injection into C57BL/6 *Lyve1*<sup>-/-</sup> or wild-  
 634 type *Lyve1*<sup>+/+</sup> mice, adoptively transferred with OT-1 transgenic T-cells. **(d)** Resulting  
 635 LN T-cell proliferation status determined by flow cytometry, plotted as percentage of  
 636 dividing OT-1 tetramer-reactive CD8<sup>+</sup> T-cells **(e)** and representative histograms of  
 637 CFSE fluorescence and CD25 expression levels within gated cell populations shown,  
 638 indicating levels of LN T-cell activation. No CD8<sup>+</sup> T-cell proliferation was detected  
 639 in non-draining LNs. Data are the mean values  $\pm$  s.e. (n = 8) from one experiment of  
 640 two, analyzed by Student's T-test. \*\*\*P < 0.005.

641 **Figure 5. DCs express HA as a cell surface coat. (a-e)** Detection of HA in CMFDA-  
 642 labeled BMDC (green), using biotinylated VG1 (bVG1) (red) following incubation in  
 643 absence (mock) or presence of hyaluronidase (HAase), shown by confocal  
 644 microscopy **(a)** and flow cytometry **(b)**, with hyaluronidase-treated control cells  
 645 (grey) and mock-treated cells (blue). Presence of HA in both BMDC lysates **(c)** and  
 646 supernatants **(d)**, both immature and following LPS-induced maturation, measured by  
 647 ELISA, (n = 15). Expression of HAS mRNA in mature DCs shown by RT-PCR **(e)**.  
 648 **(f-g)** HA on mature human CMFDA-labeled MDDCs (green) using bVG1 (red),  $\pm$   
 649 hyaluronidase, **(f)** and by flow cytometry, with hyaluronidase-treated control cells  
 650 (grey) and mock-treated cells (blue), **(g)**, with surface HA levels increasing following  
 651 LPS-induced maturation **(h)**, n = 5 from one representative experiment of three. **(i)**

652 Imaging of surface HA in endogenous dermal DCs in CD11cGFP (green) reporter  
 653 mice, detected by bVG1 (blue) and immunostained with anti-MHCeII (red),  $\pm$   
 654 hyaluronidase. (j) *Ex vivo* skin crawl-out assays showing percentage of CD11cGFP<sup>+</sup>  
 655 MHCeII<sup>+</sup> DCs retained and egressed after 24h in culture, scored as surface HA<sup>+</sup> by  
 656 microscopy, 4 mice per condition, from which three fields of view were assessed (n =  
 657 12), one experiment of three. Representative images from three separate repeated  
 658 experiments are shown. Data represent the mean  $\pm$  s.e., \*P < 0.05; \*\*\*P < 0.005;  
 659 \*\*\*\*P < 0.0001. Bar = 10 $\mu$ m.

660 **Figure 6. HA is required for efficient lymphatic migration of DCs to skin-**  
 661 **draining LNs. (a, b)** Depletion of surface HA from mature BMDCs by hyaluronidase  
 662 digestion and *in vitro* culture (72h) with 4-MU as assessed by streptavidin/bVG1  
 663 binding and flow cytometry. Graphs show surface HA levels on immature and  
 664 mature bmDC incubated either alone (mock) or in the presence of 4-MU (a) and 24h  
 665 after removal of 4-MU inhibition (b). Data are the mean  $\pm$  s.e. (BMDCs from n = 4  
 666 mice), \*\*\*\*P < 0.0001, from one experiment of three. (c-d) Trafficking of control  
 667 mock-treated and hyaluronidase/4-MU-treated BMDCs to draining LNs quantitated  
 668 by differential labelling with Q-dot655 and Q-dot585 respectively (c, upper panels) or  
 669 the reverse (lower panels), 24 h after 1:1 co-injection into the dermis of oxazolone-  
 670 treated mice. Relative numbers of each BMDC population recovered in draining LNs  
 671 are shown as dot plots and matched pair graphs (n = 5) with statistical analysis by  
 672 paired Student's t-test, with representative FACS histograms for surface HA levels in  
 673 Q-dot-labeled hyaluronidase/4-MU treated BMDCs (blue) recovered from cervical  
 674 nodes compared to mock treated controls (grey). (d) Surface HA levels graphed as the  
 675 mean  $\pm$  s.e. (pooled from samples shown in c). Data are shown from one  
 676 representative experiment of three. \*P < 0.05; \*\*P < 0.01.

677 **Figure 7. DCs adhere to LECs in an HA- and LYVE-1-dependent manner via**  
 678 **LYVE-1-enriched transmigratory cups. (a-b)** Adhesion of LPS-matured, CMFDA-  
 679 labeled BMDCs to primary mLEC monolayers after 3 h incubation in the presence of  
 680 either irrelevant rat IgG or anti-LYVE-1 mAbs B1/10, C1/8 or mAb2125 **(a)** or  
 681 following 2 h pre-incubation with hyaluronidase (HAase), **(b)**, as assessed by  
 682 fluorescence plate reader. **(c-e)** Basolateral-to-luminal transmigration of LPS-  
 683 matured, fluorescently labeled BMDCs across mLEC monolayers grown on the  
 684 undersurface of transwell filters quantitated over time by fluorescence plate reader in  
 685 the presence of irrelevant rat IgG or anti-LYVE-1 mAbs B1/10 **(c)**, C1/8 **(d)** or  
 686 mAb2125 **(e)**. Data are the mean  $\pm$  s.e., one representative experiment of three,  $n = 4$ .  
 687 \* $P < 0.05$ . **(f-h)** Confocal microscopy of cultured primary mLEC monolayers  
 688 immunostained with rabbit anti-LYVE-1 (red), viewed 3 h after addition of  
 689 fluorescently labeled BMDCs (green, CMFDA) and counter-stained with DAPI (grey,  
 690 **g-h**). LYVE-1-enriched cups surrounding individual DCs (asterisks) are indicated by  
 691 arrows, **(g, h)**, with a digital zoomed view of an orthogonal view **(i)**, (magnification:  
 692 630X, bar = 20 $\mu$ m). Representative images from three separate repeated experiments  
 693 are shown.

694 **Figure 8. LYVE-1 engagement with the HA coat on DCs is required for**  
 695 **formation of transmigratory cups. (a-c)** Quantitation of microscopy images to show  
 696 numbers of LYVE-1<sup>+</sup> cups associating with adherent DCs in mLEC monolayers  
 697 overlaid with BMDCs **(a, b)** following co-culture and incubation in the presence of  
 698 anti-mouse mAbs **(a)** or following 2 h pre-incubation with hyaluronidase (HAase), **(b)**  
 699 and in human LECs with MDDCs in the presence of the HA blocking mouse anti-  
 700 human mAb 891 **(c)**. Data represent the mean  $\pm$  s.e. ( $n = 4$ ) from one experiment of  
 701 three. **(d)** Detection of HA on endogenous dermal DCs during transmigration into  
 702 lymphatic vessels *in vivo*, in frozen skin sections from BALB/c mice subjected to

703 oxazolone hypersensitization. Sections were immunostained using bVG1 (blue), anti-  
704 MHCcIII-FITC (green) and anti-podoplanin to identify lymphatic vessels (red), bar =  
705 10µm. (e) Orthogonal view of a LYVE-1-enriched cup surrounding an individual DC,  
706 as shown in a z-stack of whole-mount mouse dermis, immunostained with rabbit anti-  
707 LYVE-1 (red), 24 h following topical application of oxazolone and intradermal  
708 injection of CMFDA-labeled BMDCs (green), magnification: 630X, bar = 20µm.  
709

## 710 **Methods**

### 711 ***Human and animal studies***

712 All studies using human tissue were approved by the Oxford Regional Health  
713 Committee (OXREC). Animal studies were performed with appropriate UK Home  
714 Office licenses with Oxford University ethical approval.

715 *LyveI*<sup>-/-</sup> mice on C57BL/6 background were kindly provided by Regeneron  
716 Pharmaceuticals NY, USA<sup>23</sup>. Mice were backcrossed for 10 generations onto a  
717 BALB/c background and subsequently maintained as a heterozygous colony at  
718 Biomedical Services, John Radcliffe Hospital. F5 TCR-transgenic mice recognizing  
719 the H-2D<sup>b</sup>-restricted influenza virus nucleoprotein epitope ASNENMDAM (Flu-  
720 NP<sub>366-374</sub>) were kindly provided by Dimitris Kioussis (National Institute of Medical  
721 Research, London, U.K.) and maintained at the Biomedical Services Unit (John  
722 Radcliffe Hospital, Oxford, U.K.). C57BL/10 and C57BL/6 mice were purchased  
723 from Envigo RMS Inc, Bicester, Oxfordshire. OT-1 C57BL/6 TCR transgenic mice  
724 recognizing the H-2K<sup>b</sup>-restricted ovalbumin epitope SIINFEKL were obtained from  
725 the Jackson Laboratory, Bar Harbor Maine, USA. CD11c-GFP reporter mice were a  
726 kind gift from Fiona Powrie (Kennedy Institute of Rheumatology, University of  
727 Oxford). All animal studies were performed with appropriate UK Home Office  
728 licenses and with approval of the Oxford local ethics committee.

### 729 ***Genotyping***

730 Ear notches from mice generated by *LyveI*<sup>-/+</sup> x *LyveI*<sup>-/+</sup> breeding were digested  
731 in 200 µl DirectPCR (Tail) lysis reagent (Viagen 102-T) supplemented with  
732 Proteinase K, 0.4 mg/ml (Sigma-Aldrich P2308) for 16 h at 55 °C, then heated to 85  
733 °C for 45 min prior to use in PCRs. MyTaq<sup>TM</sup> Red Mix (Bioline) and primers at  
734 0.8µM working concentrations were used, denaturing at 94 °C for 4 min initially,  
735 followed by 40 cycles of 94 °C for 1 min, annealing at 50 °C for 45 seconds and

736 extending at 72 °C for 45 seconds in a Hybaid PCR machine. 3' end genotyping PCR  
 737 used the primers pGK.Neo.2Fw (K/O forward primer) TCA TTC TCA GTA  
 738 TTG TTT TGC C, 3'Lyve-F3 (WT forward primer) CGT GAA AAG GTG  
 739 AGG TTG, and 161 SD (Common reverse primer) TCA CTC CTA TTG  
 740 AAC AGT ACC, yielding PCR products of 381 bp for the K/O band and 310 bp for  
 741 the WT band. 5'end genotyping PCR used the primer 161 SU (Common forward  
 742 primer) GGA GGC TTC CTT ACA TAG AC with either LACZ.SEE-RD (K/O  
 743 reverse primer) GTC TGT CCT AGC TTC CTC ACT G or 5'Lyve-R2 (WT reverse  
 744 primer) GAC AAA GGT TAG AAG GCA C, yielding products of either 556 bp for  
 745 K/O or 554 bp for WT. Products were electrophoresed on 1.2% agarose-Tris-Borate-  
 746 EDTA gels.

#### 747 ***Antibodies***

748 Rat anti-mouse LYVE-1 (mAb2125) was purchased from R & D Systems;  
 749 mAbs B1/10 and C1/8 were generated previously, using mouse LYVE-1 Fc as  
 750 immunogen<sup>28,29</sup>, as was rabbit anti-LYVE-1 polyclonal antibody<sup>20</sup>. Rat IgG fractions  
 751 were purified from hybridoma supernatants using Protein G-Sepharose. Other  
 752 antibodies were mouse anti-human LYVE-1 (R & D Systems, clone 891) and goat  
 753 anti-mouse podoplanin (R & D Systems AF3244), hamster anti-mouse podoplanin  
 754 (eBioscience 14-5381-85 clone 8.1.1), rat anti-mouse CD31 (BD Pharmingen), rat  
 755 anti-mouse VE-cadherin (BD Pharmingen), rat anti-mouse ICAM-1 (YN1/1.7.4)  
 756 (hybridoma cultured in-house, purified using Protein G-Sepharose and as used  
 757 previously in <sup>15</sup>. All antibodies were used at 10 µg/ml for immunostaining and 50  
 758 µg/ml for function-blocking. Biotinylated hyaluronan binding protein (bHABP,  
 759 recombinant human versican G1 domain, bVG-1, AMSBio, AMS.HKD-BC41) was  
 760 used at 3 µg/ml, detecting with either streptavidin-conjugated AlexaFluor 647 or  
 761 streptavidin-conjugated AlexaFluor-Pacific Blue. All secondary conjugates

(AlexaFluor 488, 546, 594, 647) were purchased from Molecular Probes, Invitrogen. Irrelevant IgG isotype controls were purchased from R & D Systems. Mouse antibodies for flow cytometry were as follows: anti-CD11c-PE/Cy7 (Biolegend 117318 clone N418), anti-CD11b-BUV395 (BD Biosciences 563553, clone M1/70), anti-MHCII (I-A/I-E)-eFluor450 (eBioscience 48-5321-82 clone M5/114.15.2), anti-CD45-BV785 (Biolegend 103149 clone 30-F11), anti-EpCAM-BV605 (Biolegend 118227 clone G8.8), anti-Langerin-PE (eBioscience 12-2075-82 clone eBioL31, anti-CD103-APC (eBioscience 17-1031-82 clone 2E7), anti-F4/80-PE/Cy5 (Biolegend 123112 clone BM8), and anti-CD86-PE (BD Pharmingen 553692 clone GL1). All antibodies that were used for functional assays (both *in vivo* and *in vitro*) were tested for endotoxin contamination using a Pierce<sup>TM</sup> LAL Chromogenic Endotoxin Quantitation kit (ThermoFisher Scientific 88282), according to the manufacturer's protocol, to ensure that endotoxin levels were less than 10 pg/ml.

## **Cells**

Primary mouse and human lymphatic endothelial cells (mLECs and hLECs) were prepared from freshly resected skin samples by immunoselection with LYVE-1 mAb and MACS<sup>®</sup> beads (Miltenyi Biotec), as described previously<sup>15</sup>. Bone marrow derived DCs (BMDCs) were extracted from tibia and fibula bones of euthanized mice, passed through a 70 µm cell strainer and cultured for 7 days in DC medium (RPMI 1640 with 10% FCS, kanamycin sulfate, MEM non-essential amino acids, sodium pyruvate, glutamine, 2-mercaptoethanol (55 mM), (all Life Technologies), and supplemented with recombinant mouse GM-CSF and IL-4 (20 ng/ml, premium grade, Miltenyi Biotec). CD11c<sup>+</sup>MHCcIII<sup>+</sup> phenotype was routinely confirmed by flow cytometry (Supplementary Fig. 4a). Human monocytes were purified from PBMCs from healthy donors by positive immunoselection using anti-CD14-conjugated MACS<sup>®</sup> beads (Miltenyi Biotec). DCs were generated by culturing monocytes for 5 days in



788 DC medium, supplemented with recombinant human GM-CSF (50 ng/ml) and 10  
789 ng/ml IL-4 (premium grade, Miltenyi-Biotec). Non-adherent DCs were matured with  
790 1 µg/ml LPS from *Salmonella abortus* (Sigma-Aldrich) and labeled with CMFDA  
791 Cell Tracker Green (Invitrogen), following the manufacturer's protocol. Jurkat E6.1  
792 cells were purchased from Sigma and tested in-house to ensure that there was no  
793 mycoplasma contamination.

794 ***Migration of DCs following oxazolone sensitization and FITC painting***

795 For measurement of endogenous dermal DC trafficking, 8 week old *Lyve1*<sup>-/-</sup>  
796 C57BL/6 or BALB/c mice or *Lyve1*<sup>+/+</sup> littermate controls were sensitized by topical  
797 application of 3% (w/v) oxazolone (4-ethoxymethylene-2 phenyl-2-oxazoline-5-one;  
798 Sigma-Aldrich E0753) + 4 mg/ml FITC (Fluorescein isothiocyanate isomer 1, Sigma-  
799 Aldrich F7250) in 95% aqueous ethanol to the shaved abdomen (150 µl/mouse).  
800 Where appropriate, anti-LYVE-1 mAbs C1/8, B1/10 or 2125 (0.5 mg/mouse) were  
801 administered by intraperitoneal (i.p) injection, 24 h prior to oxazolone and FITC  
802 painting. To assess the effects of anti-LYVE-1 mAbs on the challenge phase of  
803 contact hypersensitivity, mice were sensitized by topical application of 3% (w/v)  
804 oxazolone in 95% aqueous ethanol to both ears (50 µl/ear) on days 0 and 1, injected  
805 i.p. with mAbs on day 5, and then given a second topical application of oxazolone and  
806 FITC (0.8% oxazolone (w/v) + 4 mg/ml FITC, 150 µl/mouse) to the shaved abdomen  
807 on day 6, prior to sacrifice on day 7.

808 For trafficking of adoptively transferred BMDC, mice were sensitized and  
809 challenged with oxazolone to increase mobilization essentially as above, except  
810 oxazolone sensitization was applied to the abdomen rather than the ears and the  
811 CMFDA labeled BMDC ( $1 \times 10^6$ ) were injected intradermally at the same time as  
812 oxazolone challenge, 24h after i.p. injection of anti-LYVE-1 blocking mAbs  
813 (0.5mg/mouse) where indicated.

814 ***Ex vivo DC crawl-out assays from mouse ear explants***

815 Ears were removed from naïve mice following sacrifice, then peeled into  
816 dorsal and ventral halves and either cultured for 24 h (exposed dermis-side down) in  
817 24-well dishes in RPMI 1640 supplemented with 10% FCS, penicillin-streptomycin  
818 and glutamine (Life Technologies) and mouse TNF $\alpha$ , 50 ng/ml (R and D Systems).  
819 After culturing, dermal sheets were removed and digested in Collagenase P, (0.2  
820 mg/ml; Roche 11213865001) and Dispase, 0.8 mg/ml (Life Technologies 17105-041)  
821 in RPMI at 37 °C for 30 min, then mechanically disrupted through a 100  $\mu$ m cell  
822 strainer prior to staining alongside egressed cells for flow cytometry.

823 When investigating the effects of anti-anti-LYVE-1 mAbs on ability of DCs to  
824 egress from ear dermis, mAbs were administered to live naïve mice by i.p. injection  
825 (0.5 mg). 24 h later, mice were sacrificed and dermal sheets cultured in the presence  
826 of mouse TNF $\alpha$ , 50 ng/ml, and appropriate mAb (50  $\mu$ g/ml) for a further 24 h.

827 ***Removal of surface HA from BMDCs for adoptive transfer***

828 Non-adherent BMDCs were incubated with hyaluronidase, 15 U/ml (from  
829 *Streptomyces hyalurolyticus*, Sigma-Aldrich), for 2 h at 37 °C in DC medium, then  
830 washed and replated in DC medium supplemented with HEPES 25 mM (Life  
831 Technologies) and 4-Methylumbelliferone (7-Hydroxy-4-methylcoumarin) Sodium  
832 Salt, 4-MU (Sigma-Aldrich M1508, 0.1 mM dissolved in ddH<sub>2</sub>O) for 72 h.  
833 Maturation was induced by adding LPS 1  $\mu$ g/ml during the final 24 h incubation.  
834 Control (untreated) BMDC were mock-treated in parallel with the hyaluronidase/4-  
835 MU treated cells. Non-adherent cells were then labeled with either Qtracker<sup>®</sup> 655  
836 (Q25021MP) or Qtracker<sup>®</sup> 585 (Q25011MP) cell labeling kits, according to the  
837 manufacturer's protocol, then washed and mixed 1:1 prior to co-injection  
838 intradermally into the ears of oxazolone-sensitized mice, 0.5 x 10<sup>6</sup> cells of mock-  
839 treated and 0.5 x 10<sup>6</sup> cells hyaluronidase/4-MU treated per injection.

840 ***MVA.HIVA.NP-specific lymph node T-cell response model***

841 Lymphocytes were isolated from F5 transgenic mice and labeled with 5.5  $\mu$ M CFSE  
842 (Molecular Probes, Invitrogen), re-suspended in endotoxin-free PBS and injected  
843 intravenously into sex- and age-matched naïve C57BL/10 mice ( $2 \times 10^6$  cells/mouse).  
844 After 24 h, 0.5 mg of either rat IgG, mAb B1/10 or mAb C1/8 was administered by  
845 i.p. injection to these F5-BL10 chimeras. After another 24 h, chimeras were  
846 immunized with  $2 \times 10^6$  PFU of recombinant modified vaccinia virus Ankara  
847 expressing flu-NP<sub>366-374</sub> (MVA.HIVA.NP), intradermally, or, in the case of controls  
848 for spleen T-cell proliferation, *via* an intravenous route. mAbs were administered  
849 again 24 h after MVA.HIVA.NP injection and mice were sacrificed a further 48 h  
850 later (i.e. 3 days after MVA.HIVA.NP vaccination). Draining cervical LNs and  
851 spleens were removed and single cell suspensions obtained in FACS incubation buffer  
852 (PBS + 1% FCS, 0.01% sodium azide), then stained for NP-specific CD8<sup>+</sup> T-cells  
853 using human influenza virus A-NP<sub>366-374</sub>-specific tetramer (1/160 dilution)<sup>28</sup> and  
854 PerCP-conjugated anti-CD8 $\alpha$  mAb (1/150 dilution, BD Biosciences). Cells were  
855 washed twice in FACS buffer then resuspended in CellFix (BD Biosciences). For  
856 analysis by flow cytometry, cells were gated according to forward-scatter, side-scatter  
857 and pulse width to obtain singlets, then by detection of CD8 and NP.

858 ***Ovalbumin-specific lymph node T-cell response model***

859 CD8<sup>+</sup> lymphocytes were isolated from C57BL/6 OT-1 transgenic mice and purified  
860 by negative immunomagnetic bead selection (Miltenyi-Biotec), prior to labeling with  
861 5  $\mu$ M CFSE (Molecular Probes, Invitrogen). Cells were then washed in endotoxin-  
862 free PBS and injected intravenously into naïve sex- and age-matched C57BL/6 *LyveI*<sup>-/-</sup>  
863 mice or *LyveI*<sup>+/+</sup> littermate controls ( $4 \times 10^6$  cells/mouse). The following day,  
864 BMDCs (prepared from age- and sex-matched C57BL/6 as described above) were  
865 incubated for 1 h in the presence of ovalbumin peptide SIINFEKL ( $1 \times 10^{-7}$ M) and

866 LPS (1 µg/ml), then washed four times in PBS and injected intradermally into the ears  
867 of the OT-1 chimeras ( $0.5 \times 10^6$  BMDCs per ear). Mice were sacrificed 44 h later;  
868 draining cervical LNs and non-draining inguinal LNs were removed, passed through  
869 100 µm cell strainers to obtain single cell suspensions, then stained for OT-1-specific  
870 CD8<sup>+</sup> T-cells using tetrameric H-2 K<sup>b</sup>/OVA<sub>257–264</sub> peptide complexes conjugated with  
871 APC, anti-CD8-BV421, anti-CD25-PerCPCy5.5 and anti-CD69-PECy7, in the  
872 presence of TruStain fcX (anti-mouse CD16/CD32 clone 93, Biolegend) Fc blocker.  
873 Finally, cells were incubated with Live-Dead near-IR dead cell stain (ThermoFisher  
874 Scientific). For analysis by flow cytometry, cells were gated according to forward-  
875 and side-scatter to obtain singlets, then by detection of live dye-excluding cells, which  
876 were further characterized by expression of CD8 and detection of ovalbumin peptide  
877 by tetramer.

#### 878 ***Flow cytometric analysis of LNs***

879 LNs from either naïve or topical oxazolone-hypersensitized mice were cut into halves  
880 and digested for 37 °C in Collagenase D (Roche 11088882001), 1 mg/ml (w/v) in  
881 RPMI 1640, then mechanically disrupted through a 100µm cell strainer. Cells were  
882 suspended in incubation buffer (PBS + 10% FCS, 0.01% azide) and maintained on ice  
883 for all subsequent incubation steps. Cells were first incubated with Fixable Viability  
884 Dye eFluor780 (eBioscience 65-0865) for 15 min, then with TruStain FcX (anti-  
885 mouse CD16/CD32 clone 93, Biolegend) Fc blocker for 15 min, prior to incubation  
886 with fluorescently conjugated antibodies for 20 min. Cells were then washed and  
887 incubated for 15 min in IC Fixation Buffer (eBioscience 00-8222-49) prior to washing  
888 in Permeabilization Buffer (eBioscience 00-8333-56) and staining using anti-  
889 Langerin-PE. Staining with recombinant biotin-labeled versican G1 domain (bVG1),  
890 (Biotinylated hyaluronic acid binding protein AMS.HKD-BC41 from AMS  
891 Biotechnology (Europe) Ltd) was carried out after all other incubations, by fixing the

892 cells in 2% formaldehyde (v/v) for 5 min, then incubating with bVG1, 3 µg/ml for 40  
893 min followed by streptavidin-AlexaFluor647 (Life Technologies S21374) for 40 min.  
894 Cells were counted either manually or using 123count eBeads (eBioscience  
895 01-1234-42), and analyzed using a flow cytometer (either CyAn, Beckman Coulter, or  
896 LSRII, BD Biosciences) and using Flow-Jo software. Compensation was carried out  
897 using anti-mouse Ig/negative control compensation particle set beads (BD  
898 CompBeads 552843) and fluorescence-minus-one controls. As a control for non-  
899 specific binding of bVG1, samples were treated with hyaluronidase (see below) prior  
900 to immunostaining.

#### 901 ***Immunofluorescence antibody staining of cells and tissues***

902 Monolayers of cells cultured in 8-chamber slides (BD Falcon) were fixed in  
903 paraformaldehyde (1% w/v in PBS, pH 7.4) for 5 min, washed in PBS and then  
904 primary antibodies applied in blocking buffer (PBS + 1% BSA + 10% FCS). Cells  
905 were incubated at room temperature for 45 min, followed by washing and further  
906 incubation for 30 min with AlexaFluor secondary antibodies, prior to mounting in  
907 Vectashield+DAPI (Vector Laboratories H-1200) and viewing on a Zeiss LSM 780  
908 confocal microscope. Images were captured by sequential scanning, with no overlap  
909 in detection of emissions from each fluorophore, using either a 10X/0.3 DIC M27  
910 Plan-Apochromat (total magnification: 100x), or 40X/1.1 W Korr UV-Vis-IR LDC-  
911 Apochromat (total magnification: 400X), or 63X/1.4 oil Plan-Apochromat (total  
912 magnification: 630X, resolution: 0.24 µm).

913 For whole-mount staining, mouse dermis was fixed in 1% paraformaldehyde  
914 for 1 h, washed in PBS-Triton X-100 (0.3% v/v), blocked with BSA (1% w/v) and  
915 FCS (10% v/v) and incubated with primary antibodies at 4 °C overnight and  
916 fluorescently conjugated secondary antibodies at 2 h at room temperature. Tissue  
917 samples were then mounted in Vectashield (Vector Laboratories H-1000) and viewed

918 by confocal microscope. When staining tissue to detect transmigratory cups, tissue  
919 was left non-permeabilized, omitting Triton X-100.

920 For preparation of thin frozen sections, tissues were frozen in OCT  
921 Embedding Medium (R. A. Lamb Laboratory Supplies) before cutting 8  $\mu\text{m}$  sections  
922 by cryostat. Primary antibodies and subsequently AlexaFluor conjugates were  
923 applied, prior to mounting in Vectashield and viewing by confocal microscope.

#### 924 ***LEC-DC adhesion and transmigration assay***

925 To quantify adhesion, confluent monolayers of primary mLECs in gelatin-  
926 coated 24-well dishes were layered with  $5 \times 10^5$  fluorescently labeled LPS-matured  
927 BMDCs per well and incubated at 37 °C for 3 h. The total numbers of DCs present  
928 were then measured in a fluorescence plate reader, followed by gentle rinsing (three  
929 times with PBS) to remove non-adherent DCs, before re-measuring fluorescence and  
930 calculating the percentage of adherent cells. To assess the effect of LYVE-1 blocking  
931 mAbs the monolayers were pre-incubated (30 min, 37 °C) with LYVE-1 mAbs or  
932 control Ig as appropriate before layering with BMDCs. To remove HA from cell  
933 surfaces prior to assaying for adhesion, cells were pre-incubated with hyaluronidase,  
934 15 U/ml (from *Streptomyces hyalurolyticus*, Sigma-Aldich), for 2 h at 37 °C, then  
935 washed in medium.

936 For measurement of transmigration, primary mLECs were seeded onto the  
937 underside of gelatin-coated Fluoroblok<sup>TM</sup> cell culture inserts (3  $\mu\text{m}$  pore size, BD  
938 Falcon) and cultured in companion plates until fully confluent. Monolayers were then  
939 pre-incubated (37 °C, 30 min) with LYVE-1-blocking mAbs or control Ig as  
940 appropriate prior to the addition of  $5 \times 10^5$  fluorescently labeled LPS-matured bone  
941 marrow-derived DCs per well and transmigration assays carried out as described  
942 previously<sup>15</sup>, using a fluorescence plate reader (Synergy HT, Bio-Tek) at 37 °C.

943 ***Quantitation of LYVE-1<sup>+</sup> endothelial cup formation***

944 Primary mLECs were seeded in 8-chamber slides and cultured until confluent.  
945 Antibodies were applied 30 min before addition of  $0.1 \times 10^6$  fluorescently labeled  
946 LPS-matured BMDCs per chamber. Cells were incubated at 37 °C for 3 h then non-  
947 adherent DCs were removed by gentle washing with PBS, prior to immunostaining as  
948 detailed above. Adherent DCs from 10 fields of view per chamber were counted and  
949 scored as either alone or in association with LYVE-1<sup>+</sup> cups.

950 ***Quantitation of DC hyaluronan levels***

951 A hyaluronan ELISA kit was purchased from Echelon Biosciences and the  
952 manufacturer's protocol was followed. BMDCs were prepared from three *Lyve1<sup>+/+</sup>*  
953 BALB/c mice as described above, removing non-adherent cells to fresh tissue culture  
954 ware and culturing them for 24 h  $\pm$  LPS, (1  $\mu$ g/ml) in five replicate wells of 6-well  
955 dishes. Cells were counted and then supernatants applied directly to the assay. Cells  
956 were lysed (150  $\mu$ l/well) in lysis buffer (50 mM Tris pH 7.5, 100 mM NaCl, 1% NP-  
957 40 and 1 mM EDTA) and debris removed by centrifugation (1500 RPM, 5 min) prior  
958 to application to the assay. HA concentration was expressed in ng/ml per cell.

959 ***Characterization of mLYVE-1-HA blocking mAbs and epitope mapping***

960 For quantitative receptor binding analyses, mLYVE-1 mAbs B1/10, C1/8 and  
961 2125 (0-5 $\mu$ g/ml) were titrated individually against either soluble mLYVE-1 full-  
962 ectodomain Fc fusion protein, or Jurkat T-cells lentivirally transduced with full-length  
963 mouse LYVE-1 cDNA using a microtitre plate binding assay and flow cytometry  
964 respectively, essentially as we described previously<sup>13,46</sup>. For comparison of potencies  
965 in HA-binding blockade, the same mouse LYVE-1 lentivirally transduced Jurkat cells  
966 were subjected to high molecular weight bHA-binding assays in the presence or  
967 absence of individual mLYVE-1 mAbs (0-100 $\mu$ g/ml), detected with streptavidin  
968 Alexa485 by flow cytometry. For epitope analyses, each mLYVE-1 mAb was titrated

969 against a panel of full-length mouse LYVE-1 site-directed mutants in transfected  
970 HEK 293T cells, targeting individual amino acids equivalent to those identified as  
971 HA-binding residues in human LYVE-1 Link module, with correction for variation in  
972 surface expression and quantitation by flow cytometry<sup>30</sup>.

### 973 *Analysis of HA synthase expression by RT-PCR*

974 Total cellular RNA was isolated from LPS-matured BMDCs (RNeasy,  
975 Qiagen) and first-strand cDNA synthesis was carried out by Oligo dT priming using  
976 MMLV reverse transcriptase (Epicentre, Illumina Inc), following the manufacturers'  
977 instructions. HAS2 transcripts were amplified using the primer pair mHAS2Fwd (5-  
978 GTTTTGGTGACGACAGGCAC-3) and mHAS2Rev (5-  
979 TTCCGCCTGCCACACTTCTT-3) and MyTaq<sup>TM</sup> Red Mix PCR (Bioline),  
980 denaturing at 94 °C for 1 min, annealing at 55 °C for 2 min and extending at 72 °C for  
981 2 min. Products were resolved on 1.2% agarose Tris-Borate-EDTA gels, alongside  
982 100bp DNA ladders (New England Biolabs).

### 983 *Data and statistical analyses*

984 Data was analyzed using Excel (Microsoft) and the Mann-Whitney U test was  
985 used to compare data sets throughout this study, unless otherwise stated, using Graph  
986 Pad Prism.  $P < 0.05$  was considered significant. A computer-generated model of  
987 LYVE-1 was produced using the ModWeb program  
988 (<https://modbase.compbio.ucsf.edu/scgi/modweb.cgi>).

989





Figure 2

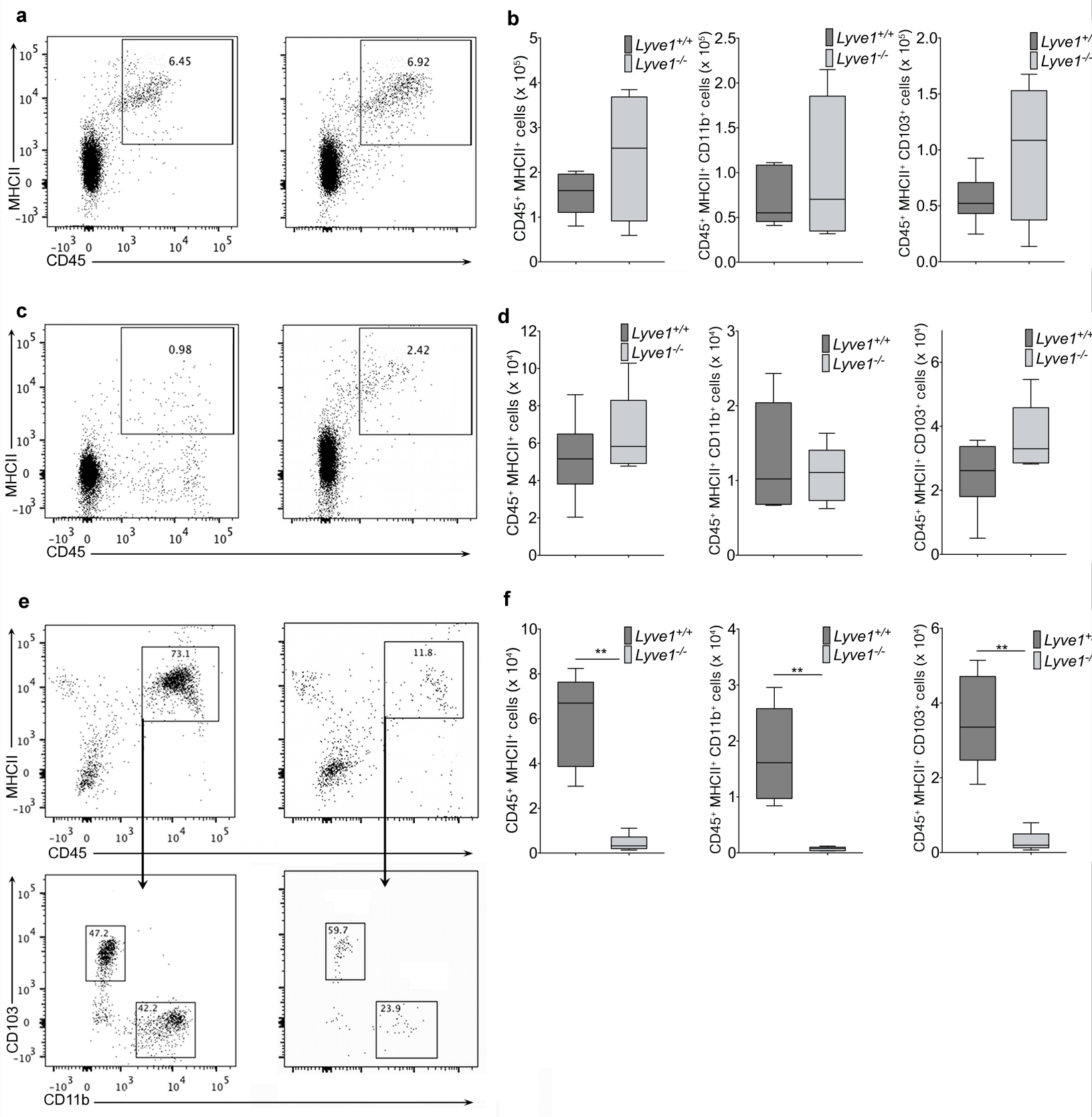


Figure 3

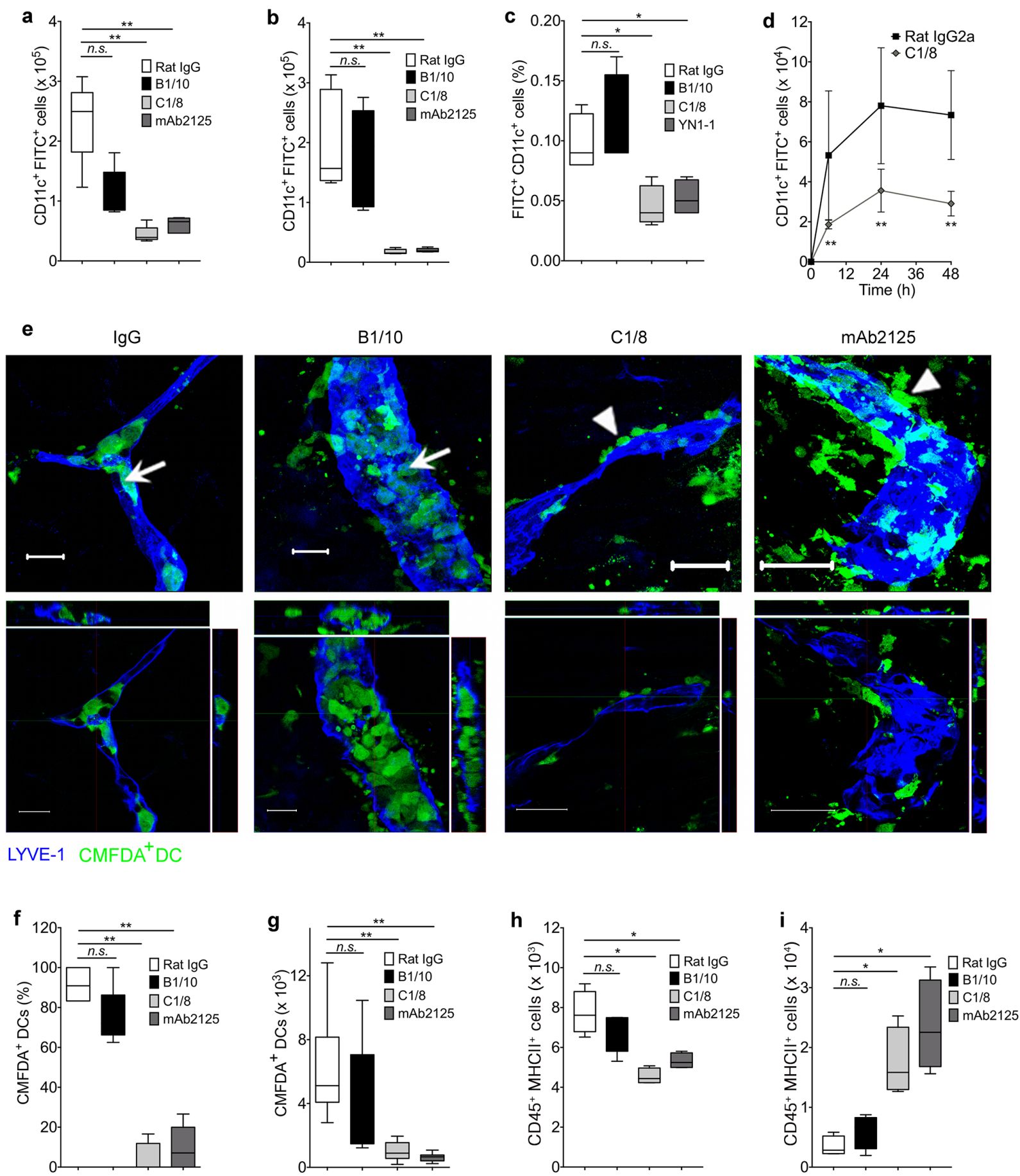
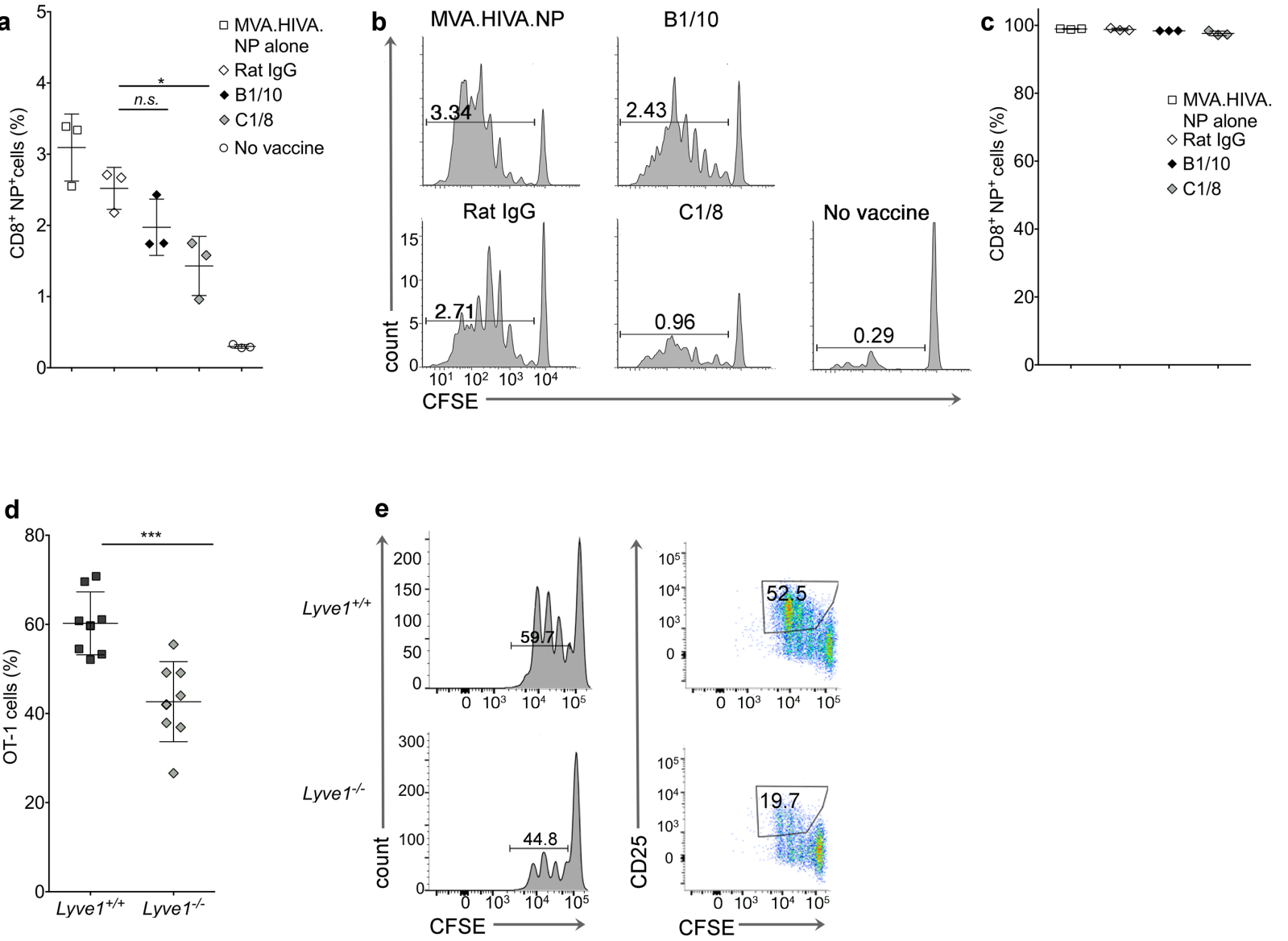
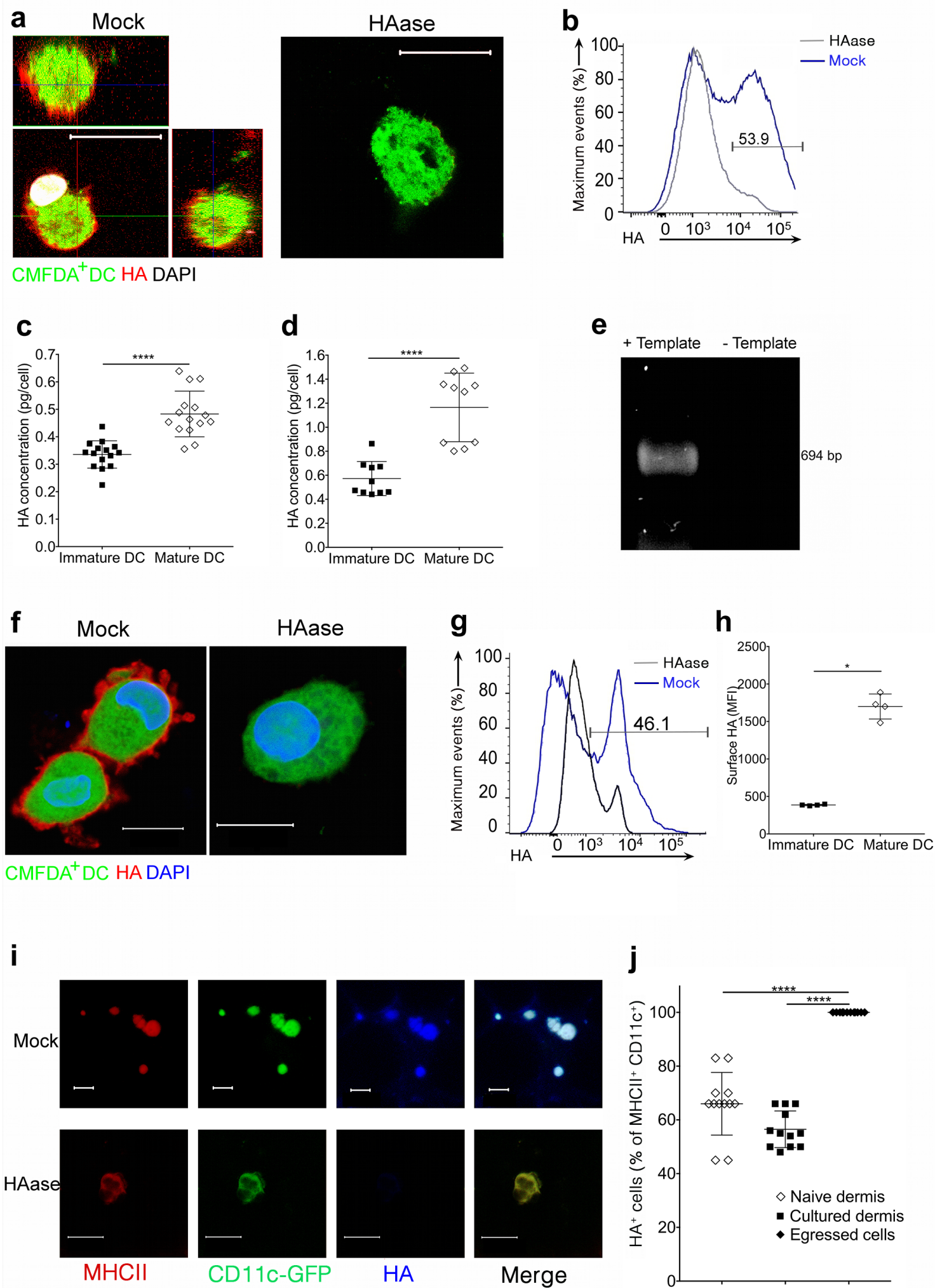


Figure 4





**Figure 5**

**Figure 6**

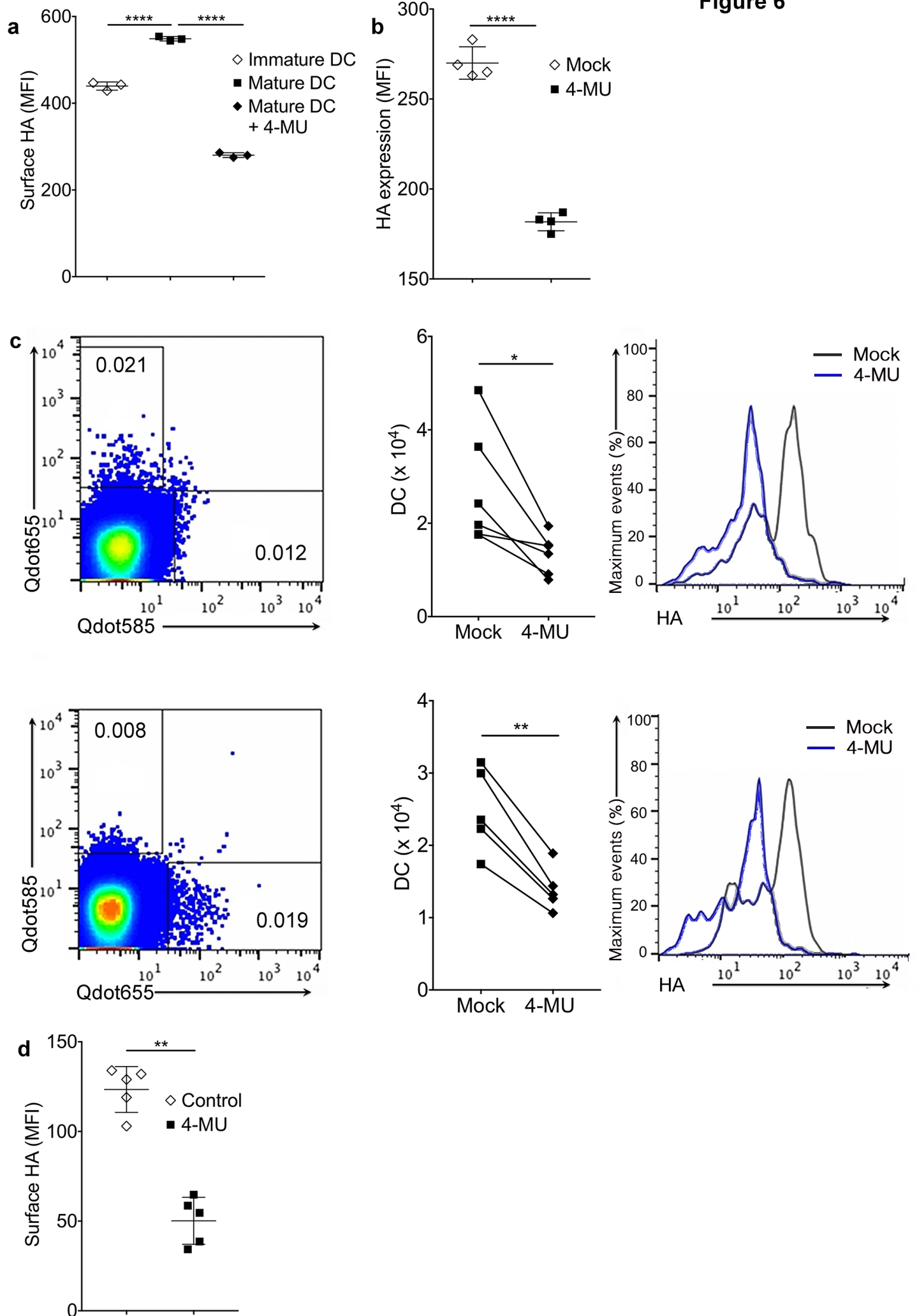


**Figure 7**

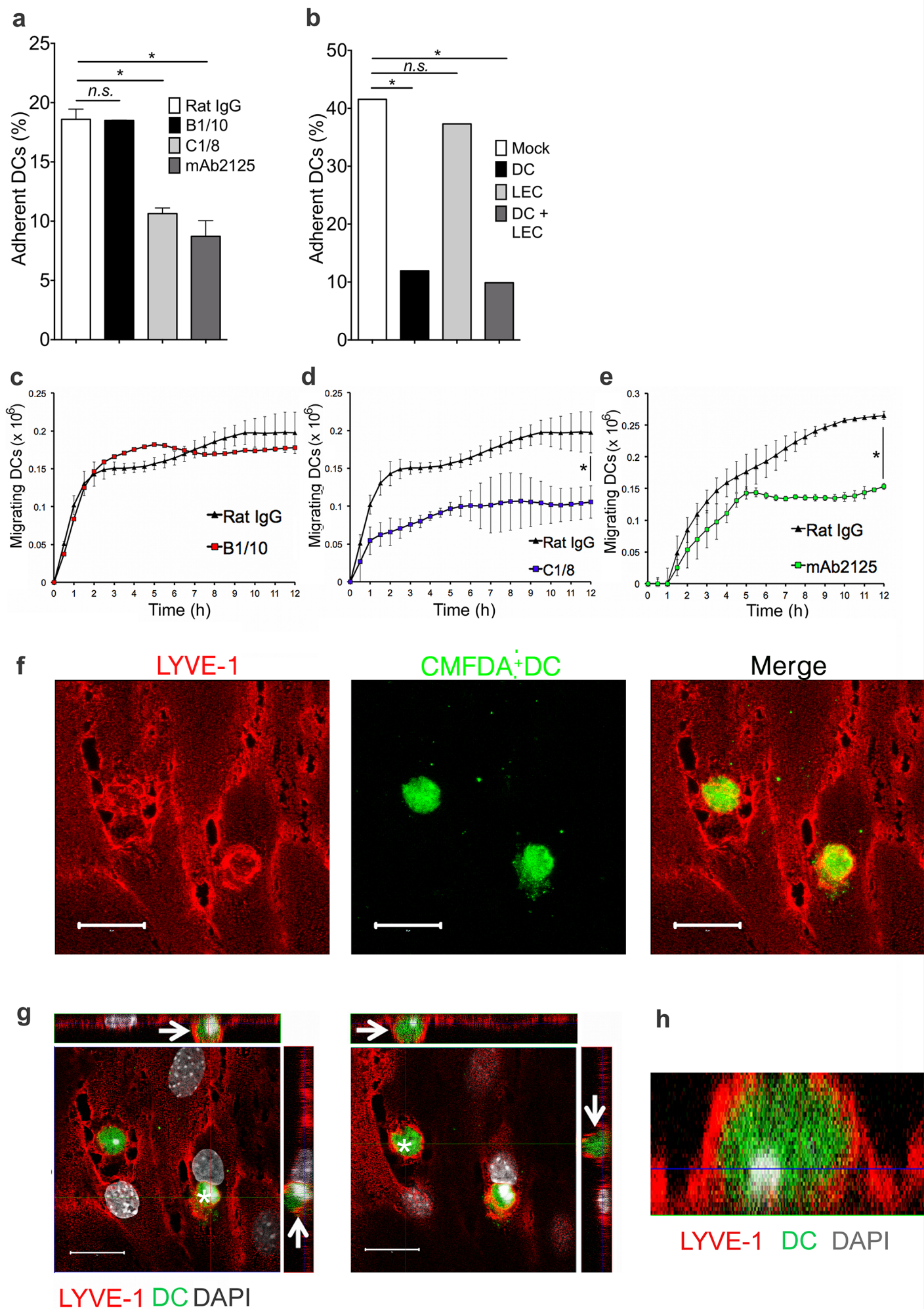




Figure 8

